Research Square

Preprints are preliminary reports that have not undergone peer review.
They should not be considered conclusive, used to inform clinical practice,
or referenced by the media as validated information.

Density measurements on (argon + carbon dioxide) over the temperature range from (253.15 to 453.15) K at pressures up to 20 MPa

Robin Wegge

robin.wegge@thga.de

Technische Hochschule Georg Agricola

Markus Richter

Leibniz University Hannover

Roland Span

Ruhr University Bochum

Research Article

Keywords:

Posted Date: November 12th, 2026

DOI: https://doi.org/10.21203/rs.3.rs-11637511/v1

License: This work is licensed under a Creative Commons Attribution 4.0 International License.
Read Full License

Additional Declarations: No competing interests reported.

Density measurements on (argon + carbon dioxide) over the temperature range from (253.15 to 453.15) K at pressures up to 20 MPa

Robin Wegge [1*], Markus Richter [2] and Roland Span [3]

[1*]GreenEnergyLab, Technische Hochschule Georg Agricola, Herner Straße 45, Bochum, 44787, Germany.
[2]Institut für Thermodynamik, Leibniz-Universität Hannover, An der Universität 1, Garbsen, 30823, Germany.
[3]Lehrstuhl für Thermodynamik, Ruhr-Universität Bochum, Bochum, 44780, Germany.

*Corresponding author(s). E-mail(s): robin.wegge@thga.de;
Contributing authors: m.richter@ift.uni-hannover.de;
roland.span@thermo.rub.de;

Abstract

The density of (argon + carbon dioxide) mixtures was measured over the temperature range from (253.15 to 453.15) K with pressures up to 20 MPa, utilizing a single-sinker densimeter adapted for measurements in gas mixtures; the apparatus and a detailed uncertainty analysis are presented. Four gravimetrically prepared mixtures with approximately (0.50 and 0.75) mole fraction carbon dioxide were investigated. The relative combined expanded uncertainty ($k = 2$) of the measured densities ranged from (0.059 to 0.127) % and (0.060 to 0.150) % for the 0.50 and 0.75 mole fraction carbon dioxide mixtures, respectively. The results are compared to experimental data from the literature and to different equations of state. The deviations from the EOS-CG-2021 [1], the current state-of-the-art multi-component mixture model for combustion-gas-like mixtures, ranged from (−2.79 to 0.19) % and (−0.53 to 0.69) %, respectively; especially at low temperatures and high pressures, systematic deviations from the equation of state were found.

Keywords: Argon, Carbon capture utilization and storage, Carbon dioxide, Density, Gas mixture, Single-sinker densimeter

1 Introduction

'Carbon Capture, Utilization and Storage' (CCUS) is one option discussed to reduce carbon dioxide emissions while satisfying the still growing global demand for energy from fossil fuels. Although CCUS-enabled systems (*e.g.*, power plants) are being operated already, technologies to realize CCUS on a large scale decrease the efficiency of the processes substantially while they require additional investment and, hence, have a negative influence on the profitability. To address this problem, the further optimization of the design and the operation of CCUS systems is necessary and, therefore, the knowledge of the thermodynamic properties of carbon-dioxide-containing mixtures is essential. Toward this end, Gernert and Span [2] developed the mixture model 'Equation of State for Combustion Gases and Combustion-Gas-Like Mixtures' (EOS-CG). Although this mixture model already describes most CCUS-relevant mixtures better than other available multi-component mixture models (*e.g.*, the GERG-2008 equation of state by Kunz and Wagner [3]), further improvements were desirable. Building on this, Neumann et al. [1] developed the EOS-CG-2021, an update and extension of the previous version that covers sixteen components of interest for CCUS processes. Experimental density and speed-of-sound data are particularly useful for the development of such models, because they allow the description of the thermal (density) and the caloric (speed of sound) properties of a substance. However, the amount of good quality experimental data for carbon-dioxide-rich mixtures is limited, and especially for (argon + carbon dioxide) mixtures hardly any density and no speed-of-sound data were available while fitting the original EOS-CG [4]. Nevertheless, the (argon + carbon dioxide) system is important in CCUS applications (*e.g.*, for oxyfuel processes) and, furthermore, a good system to evaluate the available multi-component mixture models. As first steps to provide a comprehensive set of experimental data, Wegge et al. [5] published results of speed-of-sound measurements in two (argon + carbon dioxide) mixtures over the temperature range from (275 to 500) K at pressures up to 8 MPa, and Yang et al. [6] and Ben Souissi et al. [7] published density measurements over the temperature range from (273.15 to 323.15) K with pressures up to 9 MPa.

In order to complete this data set, we investigated the (p, T, ρ, x) behavior of the (argon + carbon dioxide) system over the temperature range from (253.15 to 453.15) K and with pressures up to 20 MPa. The measurements were carried out utilizing a single-sinker densimeter; density measurements in four gravimetrically prepared mixtures containing approximately (0.50 and 0.75) mole fraction carbon dioxide were performed. We show comparisons of the measured data primarily to the EOS-CG-2021, as the current state-of-the-art multi-component mixture model for combustion-gas-like mixtures, and additionally to the GERG-2008 [3] and to the EOS-CG [2].

The EOS-CG-2021, which describes multi-component mixtures by adding up contributions from binary sub-systems, is based on the binary model of Løvseth et al. [8]. The present density data were already available during the development of that binary model and, consequently, of the EOS-CG-2021. They were, however, not used in the fitting process: no independent experimental data were available to confirm the pronounced deviations of our measurements at low temperatures and high pressures, and the developers chose to proceed without including a data set whose behavior in this region could not yet be corroborated. Including a single, as-yet unconfirmed data

set would have risked biasing the model in a region that is poorly covered by other sources.

From today's perspective, the present data still constitute the only published density measurements for the (argon + carbon dioxide) system at low temperatures and high pressures. A comparison of the EOS-CG-2021 with these data therefore provides useful information on the current state of model accuracy in this region, independent of whether the data are adopted in a future re-fit. In particular, where the EOS-CG-2021 reproduces our measurements no better than the EOS-CG, the recent update has not substantially improved the representation of these data; this points to limitations of the binary sub-model in a region that is still weakly constrained by experimental information. Further experimental data in this specific region would therefore be highly desirable.

2 Apparatus Description

The core parts of the densimeter used for the presented measurements were set up by Gedanitz [9]. Recently, Blahut et al. [10] reported density measurements on liquid squalane carried out with this device; a detailed description of the apparatus, however, has not been published so far. Furthermore, to enable measurements in (argon + carbon dioxide) mixtures, major parts of the densimeter and its instrumentation had to be rebuilt. Therefore, we describe the technical realization of this device in detail. It should be noted that the measurements presented here were carried out in the course of the doctoral work of the first author [11]. The apparatus has been modified since then; in particular, the mass and the volume of the sinker have been redetermined for the more recent measurements [10]. All specifications given in the following refer to the state of the apparatus at the time of the present measurements. The theory of the determination of fluid densities by means of the single-sinker technique will only be summarized—a comprehensive description of this measurement principle can be found in Wagner and Kleinrahm [12] and in McLinden [13]. Furthermore, Richter et al. [14] published their development of a special single-sinker densimeter for cryogenic liquid mixtures, Kleinrahm et al. [15] published a thorough analysis of the force-transmission error of single-sinker densimeters and commercial gravimetric sorption analyzers, and Yang et al. [16] recently provided a comprehensive 40-year review of the magnetic-suspension balance covering both densimetry and sorption science. As these works are the current state of the art for the single-sinker technique, the same nomenclature is used here.

2.1 Theory of the Density Measurement

The single-sinker technique is based on the Archimedes (buoyancy) principle: a fluid exerts an upward buoyancy force on an immersed sinker, which equals the weight of the displaced fluid. This principle is combined with a magnetic-suspension coupling and a load compensation mechanism; its functional principle is shown in figure 1. If a sinker of known volume V_S and mass m_S is weighed in the fluid of interest inside a

measuring cell, the weighing result, $m^*_{\mathrm{S,fluid}}$, is given by:

$$m^*_{\mathrm{S,fluid}} = m_{\mathrm{S}} - \rho_{\mathrm{fluid}} \cdot V_{\mathrm{S}}, \tag{1}$$

where ρ_{fluid} denotes the density of the fluid.

Due to a small force-transmission error of the magnetic-suspension coupling, weighing the sinker in the evacuated measuring cell (*i.e.*, at zero density) does not yield the mass of the sinker, m_{S}, but a slightly different result, $m^*_{\mathrm{S,vac}}$; in the same way, weighing the sinker in the fluid yields a slightly distorted result, $m^*_{\mathrm{S,fluid}}$. Accordingly, the density of the fluid, ρ_{fluid}, can be obtained by rearranging equation 1:

$$\rho_{\mathrm{fluid}} = \frac{m^*_{\mathrm{S,vac}} - m^*_{\mathrm{S,fluid}}}{V_{\mathrm{S}}} = \frac{\Delta m^*_{\mathrm{S}}}{V_{\mathrm{S}}}. \tag{2}$$

This equation has to be extended to account for several corrections, which are discussed later on.

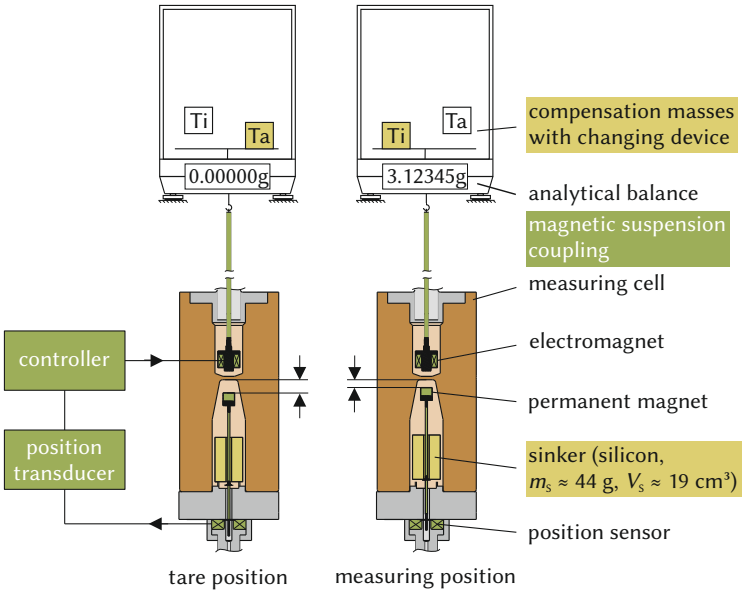


Fig. 1 Basic principle of the single-sinker densimeter.

The above-mentioned magnetic-suspension coupling consists of an electromagnet with a ferrite core, a permanent magnet, a position sensor, and a control system. The electromagnet is attached to the under-pan weighing hook of an analytical balance. The sinker (single-crystal silicon, $m_{\mathrm{S}} \approx 43.78\,\mathrm{g}$, $V_{\mathrm{S}} \approx 18.80\,\mathrm{cm}^3$, $\rho_{\mathrm{S}} \approx 2.329\,\mathrm{g\,cm}^{-3}$) and the sinker coupling and decoupling device are located in the pressure-resistant measuring cell. The permanent magnet is installed at the top part of this coupling device. At its bottom part, a position sensor is located, which allows the device's

vertical position to be determined. To couple and decouple the sinker to the balance, the permanent magnet is moved up and down, whereby two stable suspension positions can be realized—which are depicted in figure 1. In the tare position (left side in figure 1) only the coupling and decoupling device is in stable suspension. The sinker rests on the bottom of the measuring cell, and the balance is tared. To obtain the measuring position (right side in figure 1), the permanent magnet is smoothly moved upwards. The sinker is lifted by the coupling and decoupling device and, hence, attached to the balance. In this position the sinker can be weighed. To reduce the uncertainty in the weighing result, the sinker is coupled and decoupled several times. A measurement in a fluid usually consists of 15 cycles and a measurement in vacuum of 30 cycles, yielding 30 and 60 weighing results, respectively. This allows an average value with higher accuracy to be calculated. To also compensate for the zero drift, the balance is tared once at the beginning of a measurement run. The small drift in the balance reading in the tare position is taken into account by subtracting it from the reading in the measuring position throughout the measuring run.

The permanent magnet transfers most of the load to the ferrite core of the electromagnet; the coil is mainly used to change between and to stabilize the two suspension positions. This results in a nearly zero-current operation, whereby heating of the coupling housing during a measurement run is prevented largely—a necessity to maintain the thermal equilibrium.

Further systematic deviations in the weighing result may also arise from a change in the slope of the characteristic curve over the weighing range of the balance. To minimize this effect, a load compensation mechanism is applied, which ensures that the balance is operated near its tare point. Two compensation masses are alternately placed on the balance pan: (1) tare position: tantalum mass ($m_{\mathrm{Ta}} \approx 55.25\,\mathrm{g}$, $V_{\mathrm{Ta}} \approx 3.32\,\mathrm{cm}^3$, $\rho_{\mathrm{Ta}} \approx 16.65\,\mathrm{g\,cm}^{-3}$), and (2) measuring position: titanium mass ($m_{\mathrm{Ti}} \approx 15.19\,\mathrm{g}$, $V_{\mathrm{Ti}} \approx 3.38\,\mathrm{cm}^3$, $\rho_{\mathrm{Ti}} \approx 4.50\,\mathrm{g\,cm}^{-3}$). The difference of the compensation masses equals approximately the mass of the sinker, so that the total load on the balance remains constant. Since both compensation masses have nearly the same volume, the buoyancy effect of the surrounding atmosphere on the masses cancels to first order.

2.1.1 Variation of the Sinker's Volume with Temperature and Pressure

Knowledge of the exact mass and volume of the sinker is essential for accurate density measurements. The sinker's mass and volume at reference conditions ($p_0 = 1013.25\,\mathrm{hPa}$, $T_0 = 293.15\,\mathrm{K}$) were calibrated by Physikalisch-Technische Bundesanstalt [17]. The volume was determined by means of hydrostatic weighing in pentadecane to be $V_{\mathrm{S0}} = (18.79710 \pm 0.00008)\,\mathrm{cm}^3$ ($k = 2$) and the mass was determined on a high-precision mass comparator in air to be $m_{\mathrm{S}} = (43.78026 \pm 0.00012)\,\mathrm{g}$ ($k = 2$). Occasionally, the controller of the magnetic-suspension coupling fails. In this case, the electro-magnet attracts the permanent magnet strongly, accelerating the coupling device with the attached sinker. Since no safety catch is installed in the measuring cell, the permanent magnet and the sinker hit the top part of the measuring cell (a so-called crash of the magnetic-suspension coupling). This causes mechanical stress on the sinker, which can cause tiny pieces of the sinker to break off. Several of these crashes

have led to a small loss in the sinker's volume and mass. Therefore, we re-determined the volume at ambient conditions ($p_a = 1006.70\,\mathrm{hPa}$, $T_a = 295.19\,\mathrm{K}$) and the mass of the sinker by means of hydrostatic weighing in air to $V_{Sa} = (18.79700 \pm 0.00072)\,\mathrm{cm}^3$ ($k = 2$) and $m_S = (43.77970 \pm 0.00034)\,\mathrm{g}$ ($k = 2$). Since the apparatus is used over wide pressure and temperature ranges, the volume of the sinker has to be corrected for changes due to elevated pressures and temperatures over the whole (T, p) range of the device—this is done according to Richter et al. [14].

2.1.2 Force Transmission Error

As already mentioned above, the magnetic-suspension coupling is affected by a force-transmission error, which can be ascribed to two phenomena: the material of the coupling housing is not magnetically neutral and the sample fluid is always slightly diamagnetic or paramagnetic. The former can be determined by weighing the sinker in the evacuated measuring cell and by subsequently comparing the weighing result, $m^*_{S,vac}$, with the (real) mass of the sinker, m_S:

$$\epsilon_{vac}(T) = \frac{m^*_{S,vac}(T) - m_S}{m_S}. \tag{3}$$

This (relative) error ϵ_{vac} quantifies the residual magnetization of the coupling housing and is usually negligible compared to the total uncertainty of the results.

The latter (the influence of the sample fluid) originates from the slight diamagnetic behavior of most fluids. However, a few exceptions are considerably paramagnetic, namely oxygen and mixtures with oxygen (*e.g.*, (synthetic) air). These fluids can be used to determine the so-called apparatus constant, ϵ_ρ, and, subsequently, to correct for the fluid-specific effect of the force-transmission error:

$$\epsilon_{fse}(T,p) = \frac{\Delta\rho}{\rho_{fluid}(T,p)} = \epsilon_\rho \left(-\frac{\chi_s}{\chi_{s0}}\right) \cdot \left(\frac{\rho_S - \rho_{fluid}(T,p)}{\rho_0}\right), \tag{4}$$

where ρ_{fluid} is the density of the fluid and $\Delta\rho$ is the error in density due to the fluid-specific effect. Based on the results of measurements in a 0.2064 mole fraction oxygen and 0.7936 mole fraction nitrogen mixture at $T = 298.15\,\mathrm{K}$ and at pressures up to 20 MPa, we determined the apparatus constant to be $\epsilon_\rho = (0.0049 \pm 0.0010)\,\%$. χ_s is the magnetic susceptibility of the sample fluid and ρ_S denotes the density of the sinker (in this case $2329\,\mathrm{kg\,m^{-3}}$). Finally, $\chi_{s0} = 10 \times 10^{-8}\,\mathrm{m^3\,kg^{-1}}$ and $\rho_0 = 1000\,\mathrm{kg\,m^{-3}}$ are reducing constants. An empirical correction model for the force-transmission error in single-sinker densimeters and commercial gravimetric sorption analyzers, including the apparatus contribution ϵ_{vac}, the fluid-specific effect ϵ_{fse}, and the apparatus-specific constant ϵ_ρ used here, was developed by Kleinrahm et al. [15]. Further descriptions of the force-transmission error and its correction can be found in Wagner and Kleinrahm [12], McLinden et al. [18], and Richter et al. [14].

To avoid condensation of water from the (humid) ambient air on the electromagnet at low temperatures, the balance hood of the analytical balance is permanently flushed with dry nitrogen. Hence, buoyancy effects on the internal masses of the balance itself

must also be taken into account. With this effect, the force-transmission error of the coupling housing, and the fluid-specific effect, equation 2 has to be extended to:

$$\rho_{\mathrm{exp}}(T,p) = \frac{\Delta m_{\mathrm{S}}^{*}}{V_{\mathrm{S}}} \cdot \left(1 - \frac{\rho_{\mathrm{N_2}}(T_{\mathrm{a}},p_{\mathrm{a}})}{\rho_{\mathrm{ss}}}\right) \cdot \left[1 - \epsilon_{\mathrm{vac}}(T) - \epsilon_{\mathrm{fse}}(T,p)\right], \tag{5}$$

where $\rho_{\mathrm{N_2}}(T_{\mathrm{a}},p_{\mathrm{a}})$ describes the density of the nitrogen atmosphere under the balance hood at ambient pressure and temperature and ρ_{ss} denotes the density of the internal masses of the balance (made of stainless steel, $\rho_{\mathrm{ss}} = 8000\,\mathrm{kg\,m^{-3}}$).

2.2 Technical Realization of the Single-Sinker Densimeter

The schematic design of the single-sinker densimeter is illustrated by the sectional drawing in figure 2. The core apparatus basically consists of the measuring cell, the above-described magnetic-suspension coupling (manufactured by Rubotherm, Germany), a multi-layer-type vacuum thermostat with capabilities for fluid cooling (below ambient temperature) and electrical heating (above ambient temperature), and the analytical balance (Mettler-Toledo, USA, type: XP205DR; weighing range: 220 g, readability: 0.01 mg). To correct for the buoyancy on the internal masses of the balance the ambient conditions under the balance hood are monitored by a humidity and temperature transmitter (Vaisala, Finland, type: HMT330) and a barometer (Paroscientific, USA, type: 1650-101). The measuring cell is made of copper-chrome-zirconium ($\mathrm{CuCr_1Zi}$) and contains the single-crystal silicon sinker and the magnetic-suspension coupling. A six-bolt flange (made of Inconel 625, material number: 2.4856) with a gold-coated copper gasket as seal is used to close the measuring cell. This flange also incorporates the position sensor of the magnetic-suspension coupling, a sample fluid inlet port, and a sample fluid outlet port. The maximum operating pressure of the measuring cell is 30 MPa in the temperature range from (223.15 to 523.15) K. Due to the small volume of the sinker, the smallest reasonably measurable density is approximately $10\,\mathrm{kg\,m^{-3}}$ and, due to the sinker's material, the highest measurable density is approximately $2000\,\mathrm{kg\,m^{-3}}$.

2.2.1 Temperature Measurement and Control

By means of a retaining plate, the inner ring-thermostat (see figure 2) and the measuring-cell shield are attached to the upper part of the measuring cell. The cell itself is connected with a double-walled Inconel 625 tube to the base plate. The second layer of the thermostat is made up of the outer ring-thermostat and the intermediate shield. The outer ring-thermostat is also connected to the base plate of the apparatus by means of three stainless-steel tubes. Passive radiation shields are used to minimize radiant heat losses to the surrounding. Firstly, a thin aluminum sheet (wall thickness: 1 mm) is installed on the outer ring-thermostat. Secondly, a self-made multi-layer-insulation (four layers of aluminum foil between two layers of thin aluminum sheet) is attached directly to the inner surface of the vacuum insulation cylinder. The whole set-up is evacuated by means of a rotary vane pump to the order of 1 Pa.

The temperature of the measuring cell is measured by a 25 Ω capsule type standard platinum resistance thermometer (SPRT, Rosemount Aerospace, USA, type:

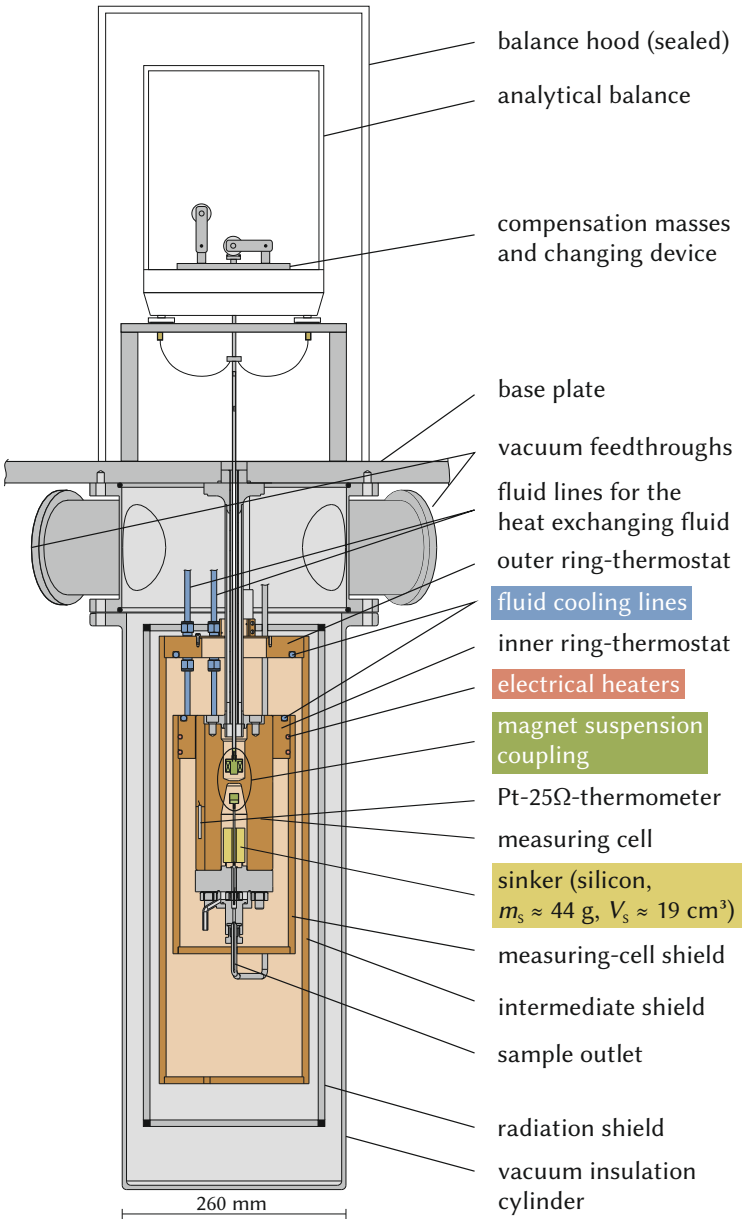


Fig. 2 Schematic design of the core apparatus of the single-sinker.

162D), which is installed in a thermometer well in the measuring-cell wall. An alternating-current resistance bridge (ASL, UK, type: F700A) is used to measure the resistance ratio between the thermometer and a 25 Ω standard resistor of Tinsley. The temperature of the intermediate shield is measured by a 100 Ω platinum resistance thermometer, which is attached to the intermediate shield. No further

thermometers are installed in the apparatus. Therefore, reliable estimations regarding temperature gradients (*e.g.*, along the measuring-cell wall) are not possible. The SPRT was calibrated at Physikalisch-Technische Bundesanstalt [19] according to ITS-90 at the triple points of mercury and water and at the melting points of gallium, indium, and tin. Afterwards, several in-house calibrations of this SPRT have been performed; the maximum shift observed at the triple point of water was less than 1.5 mK, which is well covered by the calibration contribution in the uncertainty budget of the temperature-measurement chain.

For heating the inner ring-thermostat, the measuring-cell shield, and the intermediate shield are equipped with electrical heaters. The temperature of the inner ring-thermostat and of the measuring-cell shield are controlled by a self-programmed PI controller, which regulates the output of a direct-current power supply (Agilent, USA, type: E3648A). The 25 Ω standard platinum resistance thermometer is used as control-thermometer. A commercial temperature controller (Eurotherm, UK, type: 2216e) in combination with the 100 Ω platinum resistance thermometer is used to control the temperature of the intermediate shield. Melting fuses are installed in both electrical heated parts of the thermostat. The highest maximum melting temperature of commercially available melting fuses under a continuous thermal load is T = 473.15 K. Therefore, the maximum operating temperature of the apparatus is limited to T = 453.15 K. For fluid cooling, a circulating bath (Huber, Germany, type: CC508w) with ethanol as heat exchanging fluid is used. The bath thermostat has cooling capabilities for a minimum temperature of T = 218.15 K. However, fluid cooling is only possible via two pipe coils, which are installed in the ring-thermostats. Hence, especially at low temperatures a considerable vertical temperature gradient ($\Delta T \approx 20$ K at a flow temperature of T = 230 K) over the intermediate shield can be observed, which limits the minimum temperature of the apparatus to T = 253.15 K. For steady-state operation, ethanol does not flow through the inner ring-thermostat. In both cases (fluid cooling and electrical heating), the temperature of the intermediate shield is controlled approximately 1 K below the desired set-point temperature of the measuring cell. The cell's temperature is then controlled accurately ($\sigma_T \leq 5$ mK) by means of the installed electrical heaters.

2.2.2 Pressure Measurement

For the pressure measurement, highly accurate vibrating-quartz-crystal-type transmitters of Paroscientific with a stated uncertainty of 0.01 % full scale ($k = \sqrt{3}$) are used. To achieve a sufficient measurement uncertainty in pressure of 0.01 % ($k = \sqrt{3}$) over the whole pressure range of the apparatus (in the current configuration up to 20 MPa) four transmitters with pressure ranges of (0 to 0.69) MPa, (0 to 3.45) MPa, (0 to 13.8) MPa, and (0 to 41.4) MPa are used. To decouple the devices from changes in the laboratory temperature and to achieve a supercritical temperature for carbon dioxide, the pressure transmitters are thermostated at T = 323.15 K. The pressure transmitters are not on the same geodetic altitude as the measuring cell of the densimeter, hence a hydrostatic head correction is applied. Additionally, a barometer of Paroscientific [measurement range from (0.08 to 0.11) MPa] is used to accurately determine the ambient air pressure.

2.2.3 Overview of the Total System



Fig. 3 Photograph of the densimeter in the laboratory. The key components are (from left to right): the core apparatus of the densimeter with the hooded balance at the top and the insulation cylinder containing the measuring cell at the bottom, a rack with a temperature-controlled sample manifold including pressure transmitters, and the instrument-rack.

In figure 3, a photograph of the densimeter in the laboratory can be seen. On the left side, the frame with the single-sinker densimeter is placed. The base plate stands on four height-adjustable screws on top of this frame. The vacuum insulation cylinder is installed underneath the base plate and houses the core apparatus. On top of the base plate the analytical balance with the compensation masses is placed under a sealed draft hood. To the right of this frame another frame is located, which carries the temperature-controlled sample manifold with all valves needed for the densimeter. On the backside of the plate, the four pressure transmitters are installed. Underneath the sample manifold two thermostats are placed: the bigger one (on the left side) is used for fluid cooling of the measuring cell and the smaller one (on the right side) is used to heat the sample manifold. On the right side a 19 inch instrument-rack is located, which houses all of the measurement electronics.

3 Experimental Section

Measurements on mixtures and especially on carbon-dioxide-rich mixtures impose high demands on the experimental procedures. Thereby, especially filling the measuring cell at low temperatures (*i.e.*, temperatures below the critical point of the mixture) and isobaric flushing of the measuring cell—as proposed by Richter and Kleinrahm [20] to reduce the influence of sorption effects—turned out to be difficult with the

present apparatus. Therefore, we put a special focus on these topics. Afterwards, we estimate the uncertainty of the density measurements on these mixtures according to the 'Guide to the Expression of Uncertainty in Measurement' (GUM, ISO/IEC Guide 98-3 [21]). To conduct measurements on the (argon + carbon dioxide) system over the temperature range from (253.15 to 453.15) K and pressures up to 20 MPa, two mixtures of each composition were required. We prepared all mixtures in house with a simple apparatus for the gravimetric preparation of gas mixtures. Schäfer [22] described this set-up thoroughly, hence we present the apparatus and the experimental procedures only briefly.

3.1 Experimental Procedures

Prior to the mixture measurements, we carried out test measurements on pure nitrogen at $T = (274.00,\ 295.00,\ \text{and}\ 423.15)\,\text{K}$ and pressures up to 20 MPa. The results agreed with the reference equation of state for nitrogen by Span et al. [23] within the uncertainty of the equation of state. Furthermore, we determined the apparatus-specific constant, ϵ_ρ, by measurements on a 0.2064 mole fraction oxygen and 0.7936 mole fraction nitrogen mixture (synthetic air) at $T = 298.15\,\text{K}$ and at pressures up to 20 MPa to $\epsilon_\rho = (0.0049 \pm 0.0010)\,\%$. Additionally, to determine the force-transmission error of the coupling housing, ϵ_{vac}, and the weighing result of the sinker, $m^*_{\text{S,vac}}$, over the entire temperature range of the apparatus, we recorded a vacuum-characteristic curve at six temperatures; whereby ϵ_{vac} was in the order of $-(0.0015\ \text{to}\ 0.0025)\,\%$. Nevertheless, prior to most measured isotherms additional vacuum measurements were performed to check the values for ϵ_{vac} and $m^*_{\text{S,vac}}$.

The measurements on mixtures were carried out along isotherms. Before starting the measurements, we evacuated the system thoroughly for several days by means of a turbo-molecular pump to remove any residues from preceding helium leakage tests. With the set-point temperature set to the lowest temperature ($T = 253.15\,\text{K}$), the first (argon + carbon dioxide) mixture under investigation (0.75093 mole fraction carbon dioxide) was filled into the evacuated measuring cell. Measurements started in the gas phase and, therefore, a sample cylinder with a low filling pressure (approximately 5 MPa) was used. The cell was filled to the highest desired value while ensuring that measurements were only carried out in a reasonable distance to the dew line ($p \leq 0.9 \cdot p_{\text{s}}$). As soon as the temperature of the measuring cell and the pressure of the fluid were stable within acceptable limits ($\Delta T = 2\,\text{mK}$, $\Delta p = 0.5\,\text{kPa}$), an additional 30 min were allowed before the weighings were started. As described above, for density measurements the tare and the measuring position are realized alternately by the magnetic-suspension coupling. A fluid measurement consists of 15 cycles and a vacuum measurement consists of 30 cycles. Initially, additional five cycles were used as a forerun to adjust the magnetic-suspension coupling and to improve the weighing results. However, it was discovered, that the operation of the magnetic-suspension coupling disturbs the thermal equilibrium of the measuring cell slightly. A temperature drift over the time span of a single measurement run of approximately 10 mK could be observed. To cancel this effect, the magnetic-suspension coupling was put into operation at least 1 h before starting a measurement.

3.1.1 Isobaric Flushing of the Measuring Cell

After finishing the weighings at one (T, p) state point, we flushed the measuring cell isobarically so that the sample in the system was exchanged twice with 'fresh' gas from the sample cylinder. The volume flow through the measuring cell could be monitored by means of volume-flow meters (Krohne, Germany, type: DK800/R). After re-equilibration of temperature and pressure, a new measurement run at the specific (T, p) state point was started.

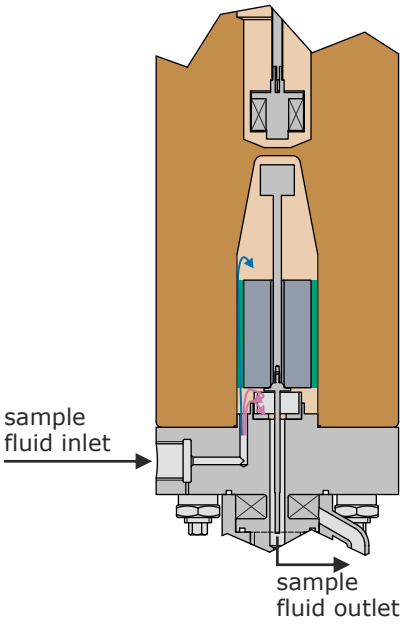


Fig. 4 Sectional drawing of the measuring cell of the single-sinker densimeter. The sinker is depicted in the measuring position. The small gap between the inner wall of the measuring cell and the outer diameter of the sinker (green colored areas) aggravates flushing of the volume above the sinker. The main flow (magenta arrows) passes directly from the inlet to the outlet port, whereas the volume above the sinker constitutes a dead-end volume that can only be exchanged slowly through the narrow gap (blue arrow).

However, we discovered that isobaric flushing of the present measuring cell, especially at high densities, is ineffective. This may be attributed to the design of the measuring cell. As illustrated by the sectional drawing in figure 4, both, the sample fluid inlet and the outlet port, are located in the six-bolt flange closing the measuring cell. Furthermore, the gap between the inner wall of the measuring cell and the outer diameter of the sinker is small (<2 mm, see green colored areas in figure 4). Hence, the main flow passes directly from the inlet to the outlet port (magenta arrows in figure 4), whereas the volume above the sinker constitutes a dead-end volume that is not traversed by the flow; it can only be exchanged with 'fresh' sample gas by diffusion and weak secondary flows through the narrow gap (blue arrow), so that the exchange is governed by the residence time rather than by the flushed volume. Even in the gas

region of the mixtures, the effect of flushing on the measured densities was small and always within the measurement uncertainty of the specific state points, indicating that major proportions of the sample fluid in the measuring cell are not exchanged during the flushing process. Consequently, at most state points isobaric flushing of the measuring cell was not performed. For future density measurements on gas mixtures, however, flushing should be enabled. It would therefore be recommendable to relocate the sample fluid outlet port from the bottom part to the top part of the measuring cell (a comparable design was realized by *e.g.*, Richter et al. [14]), thus forcing the 'fresh' sample to flow through the entire measuring cell.

After finishing the measurements at a specific state point, further isothermal (T, p) state points at lower pressures followed, until the minimum pressure of 1 MPa was reached. Measurements below that pressure are generally possible, but the usually low density at low pressures leads to a high relative measurement uncertainty.

Before increasing the temperature to reach the next isotherm, the sample was vented to approximately 0.1 MPa. As soon as the desired temperature was stable, the system was evacuated for at least 24 h and vacuum measurements were performed to check the values for ϵ_{vac} and $m^*_{\mathrm{S,vac}}$. After finishing the measurements in the gas phase of the (argon + carbon dioxide) mixture with 0.75093 mole fraction carbon dioxide, measurements in the liquid phase and in the supercritical fluid followed. Therefore, another sample cylinder (0.74985 mole fraction carbon dioxide, filling pressure approximately 20 MPa) was attached to the sample manifold. Again, the system was thoroughly evacuated and with the set-point temperature set to the lowest value (253.15 K) the measuring cell was pressurized.

3.1.2 Filling the Densimeter at Low Temperatures

The results of the first isotherm of the mixture with 0.74985 mole fraction carbon dioxide (T = 253.15 K, p = (14 to 20) MPa, see left-pointing triangles in figure 5) showed very large deviations of (−4.83 to −2.66) % compared to the EOS-CG-2021 of Neumann et al. [1]. To investigate the reason for these large deviations, after the last measured (T, p) state point (at p = 14 MPa) the sample was not vented, but the measuring cell was successively re-pressurized to perform a reproducibility test (see right-pointing triangles). Thereby, the course of the measured values was comparable, but large offsets of up to 1.3 % could be observed.

The most probable explanation for these results is a decomposition of the mixture during the filling procedure. In the upper part of figure 6, the filling process of the evacuated measuring cell is depicted in a (p, h) diagram. The pressure of the fluid in the sample cylinder is approximately 20 MPa and the cylinder is heated to approximately T = 323.15 K (see point 1 in figure 6). The expansion of the mixture from the supercritical state inside the sample cylinder into the evacuated measuring cell is isenthalpic and, thus, the fluid will be expanded into the two-phase region (point 2). Generally, the measuring cell is pressurized slowly to avoid damaging the sinker. Hence, there is enough time for the fluid to equilibrate at low pressures and decompose into two phases.

After filling the measuring cell to the final pressure, the fluid is again in a homogeneous state (point 3). Nevertheless, filling the measuring cell through the two-phase

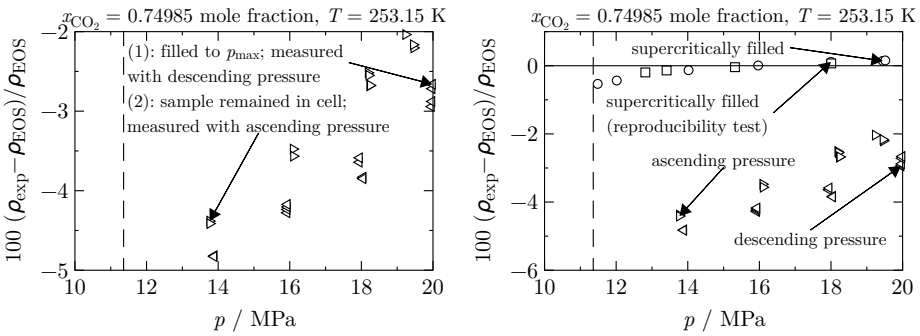


Fig. 5 Results of density measurements on an (0.25015 argon + 0.74985 carbon dioxide) mixture at T = 253.15 K. Relative deviations of experimental densities, ρ_{exp}, from values, ρ_{EOS}, calculated with the EOS-CG-2021 of Neumann et al. [1] are plotted versus pressure, p. ◁, standard filling procedure—measured with descending pressure; ▷, reproducibility test for the standard filling procedure—measured with ascending pressure; ○, supercritical filling procedure—run 1; □, supercritical filling procedure—run 2 (reproducibility test); - -, phase boundary.

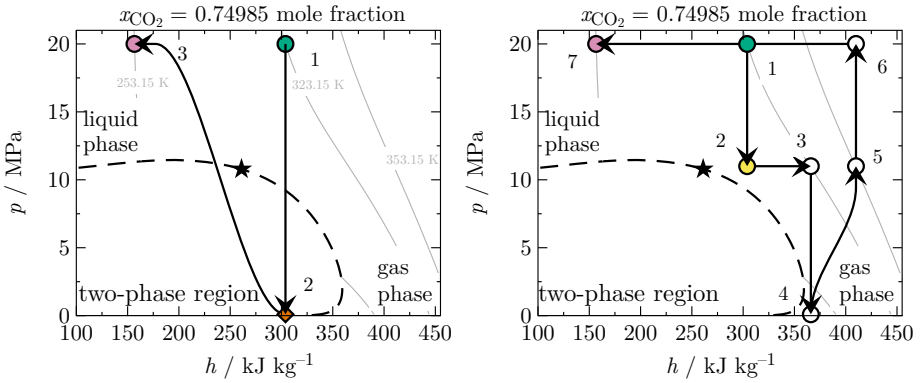


Fig. 6 (p, h) diagrams with phase boundaries (dashed lines) of an (argon + carbon dioxide) mixture (0.74985 mole fraction carbon dioxide) investigated in this work. The phase boundaries and the isotherms (thin gray lines; temperatures as labeled in the left panel) were calculated with the EOS-CG-2021 of Neumann et al. [1]; ★, critical point. In the left panel, the standard filling procedure is depicted; in the right panel, the supercritical filling of the measuring cell is shown. The thick black paths with arrows indicate the course of the respective filling procedure, with the numbered states explained in the text; green circles mark the state of the heated sample cylinder (state 1), pink circles the final state in the measuring cell (states 3 and 7, respectively), and open circles intermediate states. The orange diamond (state 2, left panel) marks the state within the two-phase region at which the slowly pressurized sample decomposes, whereas the yellow circle (state 2, right panel) marks the state reached by the abrupt pressurization of the sample manifold, at which no decomposition occurs.

region leads to a shift in composition, because complete remixing of the fluid in the cell cannot be taken for granted. By re-pressurizing the measuring cell to perform the reproducibility test with ascending pressure (right-pointing triangles in figure 5), the amount of sample with the 'correct' composition is increased and, hence, the deviation compared to the equation of state decreases.

To avoid this shift in composition, a supercritical filling procedure is required. It should be noted that for a fully supercritical filling procedure, as performed by Richter et al. [14], the sample cylinder and all parts in contact with the sample fluid must be heated to a temperature greater than 353.15 K, which is not possible with the current set-up. Hence, specifically for the mixtures containing 0.75 mole fraction carbon dioxide, the fluid will at some point cross the phase boundary during the expansion. Nevertheless, it is possible to avoid a decomposition of the mixture, if the volume of the pressurized system is small (a few mL) and pressurizing happens abruptly ($\Delta p/\Delta t \approx 5\,\mathrm{MPa\,s^{-1}}$).

In the second (p, h) diagram of figure 6 the supercritical filling procedure is depicted. Crucial for this procedure is, that the measuring cell is heated to $T = 353.15\,\mathrm{K}$. Starting from the heated sample cylinder (point 1), the sample is expanded isenthalpically, but this time only the sample manifold is pressurized, and the inlet valve to the measuring cell remains closed. Thus, only a small volume[1] has to be pressurized and, furthermore, abrupt pressurization of the sample manifold is possible (in this example to a pressure of approximately 11 MPa in approximately 3 s). Hence, the sample has not enough time to equilibrate at low pressures and will not decompose (point 2 in the right diagram of figure 6). After filling the sample manifold, 15 min equilibration time is allowed, in which the sample is heated to $T = 323.15\,\mathrm{K}$ (the temperature of the sample manifold, point 3 in figure 6). Subsequently, the inlet valve to the evacuated and heated measuring cell ($T = 353.15\,\mathrm{K}$) is opened (point 4) and the system is pressurized to the filling pressure of the sample manifold; depicted by point 5 in figure 6. Afterwards the pressure can be increased to the maximum filling pressure of 20 MPa (see point 6) and the cell can be cooled down isobarically to the desired temperature (in this example $T = 253.15\,\mathrm{K}$, see point 7). Therefore, the valve of the sample cylinder must remain open until the measuring cell is at the desired temperature. This procedure could be further improved by integrating a heat exchanger into the filling line, by which the flowing fluid could be superheated to temperatures of the order of $T = 373.15\,\mathrm{K}$. This would allow direct filling of the cooled, evacuated measuring cell.

An additional test we performed was to fill the cooled cell at first with pure argon to a pressure of approximately 13 MPa and then pressurize the cell to 20 MPa with the mixture under study—thus preventing decomposition of the mixture. Subsequently, we tried to flush out the argon with the mixture sample. However, even after exchanging the internal volume of the cell more than ten times with 'fresh' gas from the sample cylinder, the deviations from the EOS-CG-2021 remained in the order of −50 %, which is a further validation of the assumption that the design of the present measuring cell does not enable isobaric flushing.

Utilizing the supercritical filling procedure, another two measurement runs at $T = 253.15\,\mathrm{K}$ and in the pressure range from (12 to 20) MPa were performed (see circles and squares in the right panel of figure 5). For the reproducibility test, the sample in the cell was vented, the cell was heated to $T = 353.15\,\mathrm{K}$, and the described filling

[1] The inner volume of the pressurized part of the sample manifold is estimated to be 20 mL, which is substantially smaller than the inner volume of the measuring cell (approximately 80 mL), and it does not contain narrow flow paths like those constituted by the gap between the sinker and the measuring-cell wall (see figure 4).

procedure was repeated. As a result, the deviation from the EOS-CG-2021 is much smaller, and the offset between both series of measurements lies within the uncertainty of the present measurements. Hence, the supercritical filling procedure allows the apparatus to be filled reproducibly, avoiding decomposition of the sample.

The increased amount of argon facilitated the handling of the 0.50 mole fraction carbon dioxide mixtures and decomposition of the mixtures during filling of the apparatus was not a problem. Because of the high thermal mass of major parts of the vacuum thermostat, the measurements for these mixtures started at the highest set-point temperature and temperatures were decreased for subsequent isotherms. This helped to limit the overall time needed for the measurements in the (argon + carbon dioxide) mixtures. Again, two samples with different filling pressures were used for gas-phase measurements (0.50000 mole fraction carbon dioxide, filling pressure approximately 5 MPa) and for the measurements in the liquid phase and in the supercritical region (0.49975 mole fraction carbon dioxide, filling pressure approximately 18 MPa).

3.2 Gravimetrical Preparation of the Gas Mixtures

The specific binary mixtures investigated here were prepared gravimetrically utilizing the apparatus for the gravimetrical preparation of gas mixtures, described thoroughly by Schäfer [22]. Pure substances as listed in table 1 were used as received. No further purification was attempted and no gas analysis was conducted to confirm the stated purities.

Table 1 Purities of the pure substances used for the gravimetrical preparation of the gas mixtures.

Substance	**Source**	**Purity / volume fraction**
argon	Air Liquide, France	0.999990
carbon dioxide	Air Liquide, France	0.999995

Aluminum cylinders (Scott Specialty Gases, Netherlands) with aculife III and IV treatment and an internal volume of 20 L were used as sample cylinders. As part of the aculife treatments, the inner surface of the cylinders is chemically polished by the manufacturer. Furthermore, the cylinders are baked out several times, evacuated to a very low pressure, and purged with nitrogen to remove residual components, especially water. Consequently, prior to the preparation of the mixtures, the cylinders were thoroughly evacuated for 24 h by means of a turbo-molecular vacuum pump. Subsequently, the weight of the evacuated cylinder was determined accurately by means of a mass comparator (Sartorius, Germany, type: CCE60K3; weighing range: 64 kg). Therefore, the balance was tared and its reading with the empty weighing pan was recorded. Then, the cylinder was placed on the weighing pan and the balance reading was recorded again. A load-centering mechanism, a so-called centermatic (Sartorius, Germany, type: YWP03C), helped to ensure that the mass center of the cylinder was

placed properly on the center of the balance. To reduce the uncertainty of the weighing result, this procedure was repeated ten times. Thereby, the balance was tared once at the beginning of the procedure so that the small drift in the balance reading with the empty weighing pan is taken into account by subtracting it from the reading with the sample cylinder placed on the balance. To compensate for the air buoyancy on the cylinder, the temperature and the humidity of the ambient air are observed by means of a humidity and temperature transmitter (Vaisala, Finland, type: HMT330). Furthermore, the air pressure is measured with a barometer (Paroscientific, USA, type: 1650-101).

Afterwards, the sample cylinder and the supply cylinder were connected to a sample manifold, whereby the sample cylinder remained on the weighing pan of the balance. The sample lines were purged several times with 'fresh' gas and, starting with carbon dioxide, the sample was slowly introduced into the cylinder until the pre-calculated target mass was reached. The sample cylinder was then disconnected from the manifold. An equilibration time of 6 h was allowed, so that the sample cylinder could re-adjust to the ambient temperature. Afterwards the actual mass of the filled-in fluid was determined, applying the above-described weighing scheme. This procedure was repeated for the second component (argon).

Table 2 Gravimetric compositions (mole fraction), average molar mass, M, and uncertainty in composition, $U(x_{\mathrm{CO_2}})$ ($k = \sqrt{3}$), of the studied mixtures. Mixtures (1a) and (1b) contain approximately 0.50, mixtures (2a) and (2b) approximately 0.75 mole fraction CO_2.

Component	**(1a)**	**(1b)**	**(2a)**	**(2b)**
argon	0.500 00	0.500 25	0.249 07	0.250 15
carbon dioxide	0.500 00	0.499 75	0.750 93	0.749 85
M / g mol^{-1}	41.979	41.978	42.998	42.994
$U(x_{\mathrm{CO_2}})$ ($k = \sqrt{3}$)	2.5×10^{-5}	2.7×10^{-5}	2.2×10^{-5}	2.0×10^{-5}

For the density measurements carried out in this work, four gas mixtures were prepared; the compositions of the mixtures and the uncertainties in compositions (estimated according to Schäfer [22]) are listed in table 2. The sample cylinders for mixtures 1a and 2a were loaded to 5.5 MPa and 5.1 MPa, respectively. Thus, measurements in the gas phase of the mixtures could be performed easily without crossing the phase boundary while filling the apparatus. The cylinders for mixtures 1b and 2b were loaded to 18.3 MPa and 19.8 MPa, respectively.

3.3 Uncertainty Analysis

We estimated the combined standard uncertainty of density measurements $u_{\mathrm{c}}[\rho(T,p)]$ according to the 'Guide to the Expression of Uncertainty in Measurement' (GUM, ISO/IEC Guide 98-3 [21]). At first we describe the determination of the standard uncertainty of the density measurement, $u_{\mathrm{c}}[\rho(T,p)]$. In a second step we integrate the

mixture uncertainty into this uncertainty analysis, so that the combined uncertainty for density measurements in (argon + carbon dioxide) mixtures, $u_c[\rho(T,p,x)]$, can be obtained.

3.3.1 Uncertainty of the Density Measurement

To obtain the standard uncertainty of density measurements $u_c[\rho(T,p)]$ influences arising from different sources have to be considered:

- At first, the uncertainty, $u(\rho)$, arising from the determination of the density itself has to be considered. This includes the contributions from the analytical balance, the correction of the air buoyancy on the internal weights of the balance, from the description of the volume of the sinker, and from the estimation of the force-transmission error and the associated corrections.
- A further source of uncertainty is the temperature-measurement chain $[u(T)]$, including the contributions from the thermometry bridge, the SPRT, and the reference resistor. Furthermore, temperature gradients along the measuring-cell wall, oscillations in temperature over time, the self-heating of the sensor, heat dissipation of the test leads, and the calibration of the temperature-measurement chain have to be considered.
- And finally, the uncertainty of the pressure-measurement chain, $u(p)$, has to be taken into account. In this work, this contribution consists of the uncertainties for the pressure transmitters as given by the manufacturer and the uncertainty of the hydrostatic head correction.

Assuming that these quantities are not correlated, the uncertainty in density measurement can be estimated by:

$$u_c[\rho(T,p)] = \sqrt{u(\rho)^2 + \left[\left(\frac{\partial\rho}{\partial T}\right)_p u(T)\right]^2 + \left[\left(\frac{\partial\rho}{\partial p}\right)_T u(p)\right]^2}. \tag{6}$$

Determination of Density

The contribution of the analytical balance to the uncertainty of the determination of the density $u(\rho)$ arises from the non-linearity of the characteristic curve over the weighing range (1.2×10^{-5} g), the sensitivity drift (1.0×10^{-5} g), and the repeatability in the fine range (1.8×10^{-5} g). The values are calculated based on equations given by the manufacturer and with a maximal net and gross weight of (13 and 93) g, respectively, which were encountered in the measurements on the (argon + carbon dioxide) system at low temperatures and high pressures. The values are assumed to be rectangularly distributed ($k=\sqrt{3}$). Furthermore, the buoyancy on the internal weights of the balance needs to be compensated for. Therefore, the temperature and relative humidity under the balance hood are measured by means of a humidity and temperature transmitter (uncertainty: 0.2 K and 1 % relative humidity, for both values: $k=\sqrt{3}$). The pressure under the balance hood is measured by a barometer (uncertainty: 0.11 hPa, $k=\sqrt{3}$). Furthermore, the uncertainty in mass of the internal weights of the balance

is 1 % ($k = \sqrt{3}$). Based on these influences, the uncertainty of the air-buoyancy correction can be estimated to be 0.0050 % ($k = 1$). A further contribution to the uncertainty of the density measurement derives from the determination of the volume of the sinker at reference conditions. The volume was calibrated by the Physikalisch-Technische Bundesanstalt [17] with a very high accuracy of 0.00008 cm^3, which would correspond to 0.0004 % ($k = 2$). However, due to several crashes of the magnetic-suspension coupling tiny pieces broke off the sinker. Therefore, we re-determined the volume of the sinker with an uncertainty of 0.00072 cm^3, which corresponds to 0.0040 % ($k = 2$). Additionally, the descriptions of the variation of the sinker's volume with temperature and pressure are not exact. In accordance with the relations given by Richter et al. [14], the uncertainty of the temperature correction in the investigated (T, p) range is estimated to be 0.0022 % and the uncertainty of the pressure correction in the investigated (T, p) range is estimated to be 0.0034 % (both, $k = \sqrt{3}$). The average standard deviation of the weighing of the sinker in fluids and in vacuum is also considered as an uncertainty contribution. For the measurements performed here the uncertainty contribution for both cases was found to be 0.05 mg (uncertainty distribution: Student's t). The last contribution arises from the determination and the correction of the force-transmission error. This error was estimated to be 0.0050 % ($k = 1$). All uncertainty contributions relevant for the determination of the density are listed in table 3.

Temperature-Measurement Chain

In comparison to the original set-up of Gedanitz [9], the temperature measurement chain of the single-sinker densimeter was not modified. However, it was not possible to verify the comparably low values for *e.g.*, the temperature-gradients given by Gedanitz [9]. Therefore, for the carried out measurements we revised the uncertainty assessment for the temperature-measurement chain of Gedanitz [9] ($U(T) = 6$ mK, $k = 2$) according to our experience with other comparable experimental devices. Being more conservative, the uncertainty contribution arising from temperature gradients over the measuring-cell wall is estimated to be 10 mK and the contribution arising from the oscillations over time is estimated to be 5 mK (both, $k = \sqrt{3}$). Finally, the expanded combined uncertainty in temperature measurement has to be estimated to be 17 mK ($k = 2$). All individual values for the different contributions to the standard uncertainty in temperature $u(T)$ are listed in table 4.

Pressure-Measurement Chain

The uncertainty in pressure measurement $u(p)$ mainly depends on the uncertainty of the vibrating-quartz-crystal-type pressure transmitters. The manufacturer specifies the uncertainty to be $u(p) = 0.010\,\%\ p_{\max}$ ($k = \sqrt{3}$), whereby $p_{\max}$ corresponds to the maximum pressure of the respective pressure transmitter. Generally, it would be necessary to account for the uncertainty of the hydrostatic head correction. However, this contribution is very small compared to the other influences and, therefore, it can be neglected. The uncertainty contributions of the available pressure transmitters are listed in table 4.

Table 3 Budget for the uncertainty of the density measurement, $u(\rho)$.

Source of uncertainty	Uncertainty	Distribution	Sensitivity coefficient	Standard uncertainty
Standard deviation of the weighing of the sinker in the fluid	0.150 mg	Student's t	$1/V_{\mathrm{Sa}}$	0.0080 $\mathrm{kg\,m^{-3}}$
Standard deviation of the weighing of the sinker in vacuum	0.020 mg	Student's t	$1/V_{\mathrm{Sa}}$	0.0011 $\mathrm{kg\,m^{-3}}$
Linearity of the characteristic curve	0.150 mg	Rectangular	$1/V_{\mathrm{Sa}}$	0.0080 $\mathrm{kg\,m^{-3}}$
Sensitivity drift	0.030 mg	Rectangular	$1/V_{\mathrm{Sa}}$	0.0016 $\mathrm{kg\,m^{-3}}$
Repeatability in the fine range	0.020 mg	Rectangular	$1/V_{\mathrm{Sa}}$	0.0011 $\mathrm{kg\,m^{-3}}$
Air-buoyancy correction	0.002 mg	Normal	$1/V_{\mathrm{Sa}}$	0.0001 $\mathrm{kg\,m^{-3}}$
Force-transmission error	0.700 mg	Normal	$1/V_{\mathrm{Sa}}$	0.0372 $\mathrm{kg\,m^{-3}}$
Sinker's volume at reference conditions	0.720 $\mathrm{mm^3}$	Normal, ($k = 2$)	$\Delta m_{\mathrm{S}}^{*}/V_{\mathrm{Sa}}^{2}$ [a]	0.0143 $\mathrm{kg\,m^{-3}}$
Temperature correction of the sinker's volume	0.140 $\mathrm{mm^3}$	Rectangular	$\Delta m_{\mathrm{S}}^{*}/V_{\mathrm{Sa}}^{2}$ [a]	0.0055 $\mathrm{kg\,m^{-3}}$
Pressure correction of the sinker's volume	0.002 $\mathrm{mm^3}$	Rectangular	$\Delta m_{\mathrm{S}}^{*}/V_{\mathrm{Sa}}^{2}$ [a]	0.0008 $\mathrm{kg\,m^{-3}}$

[a] $\Delta m_{\mathrm{S}}^{*}$ varies with each individual (T, p) state point—the displayed standard uncertainties represent the maximal values in the measured (T, p) range.

Table 4 Budgets for the uncertainty of the temperature-measurement chain, $u(T)$, and the pressure-measurement chain, $u(p).$

Source of uncertainty	Uncertainty	Distribution	Sensitivity coefficient	Standard uncertainty
Temperature-measurement chain				
A/C resistance bridge	1.0 mK	Rectangular	$(\partial\rho/\partial T)_p$ [a]	$c_T \cdot$ 0.6 mK
Calibration of the thermometer	4.0 mK	Normal	$(\partial\rho/\partial T)_p$ [a]	$c_T \cdot$ 4.0 mK
Calibration of the standard resistor	4.0 mK	Normal	$(\partial\rho/\partial T)_p$ [a]	$c_T \cdot$ 4.0 mK
Temperature gradients	10.0 mK	Rectangular	$(\partial\rho/\partial T)_p$ [a]	$c_T \cdot$ 5.8 mK
Oscillations over time	5.0 mK	Rectangular	$(\partial\rho/\partial T)_p$ [a]	$c_T \cdot$ 2.9 mK
Pressure-measurement chain				
Pressure transmitter 1 ($p_{\max} = 41.1\,\mathrm{MPa}$)	41.1 hPa	Rectangular	$(\partial\rho/\partial p)_T$ [a]	$c_p \cdot$ 23.9 hPa
Pressure transmitter 2 ($p_{\max} = 13.8\,\mathrm{MPa}$)	13.8 hPa	Rectangular	$(\partial\rho/\partial p)_T$ [a]	$c_p \cdot$ 7.97 hPa
Pressure transmitter 3 ($p_{\max} = 3.45\,\mathrm{MPa}$)	3.45 hPa	Rectangular	$(\partial\rho/\partial p)_T$ [a]	$c_p \cdot$ 2.00 hPa
Pressure transmitter 4 ($p_{\max} = 0.69\,\mathrm{MPa}$)	0.69 hPa	Rectangular	$(\partial\rho/\partial p)_T$ [a]	$c_p \cdot$ 0.40 hPa

[a] Calculated for each individual (T, p) state point with the EOS-CG-2021 of Neumann et al. [1].

Sensitivity Coefficients

The uncertainty contributions of the temperature- and the pressure-measurement chain depend on the state of the individual measured (T, p) point. The sensitivity coefficients, $(\partial\rho/\partial T)_p$ and $(\partial\rho/\partial p)_T$, in equation 6 account for this dependence. For the present measurements the partial derivatives can be calculated with sufficient accuracy with the EOS-CG-2021 of Neumann et al. [1]. The density measurements on the (argon + carbon dioxide) system carried out in this work cover a large pressure, temperature, and density range with four different mixture compositions. Hence, to not further complicate the representation of the uncertainties in table 3, no overall uncertainty is given. Nevertheless, the combined standard uncertainty is discussed below, and the numerical value for each measurement point is listed together with the thermal properties in tables 5 and 6.

3.3.2 Uncertainty for Density Measurements in Mixtures

The estimation of the influence of the uncertainty of the mixture composition on the measured density of the fluid is complex, because the changes in composition of the individual components are correlated.

The contribution of the mixture composition to the uncertainty of the present density measurements was estimated following the approach proposed by Richter et al. [14] for measurements in liquid mixtures, where no sorption effects will occur. For a binary mixture, their multi-component approach reduces to:

$$u[\rho(x)] = u[\rho(x_{\mathrm{CO_2}})] = \sqrt{\left(\frac{\Delta\rho}{\Delta x_{\mathrm{CO_2}}} u(x_{\mathrm{CO_2}})\right)^2}. \tag{7}$$

Thereby $u(x_{\mathrm{CO_2}})$ corresponds to the uncertainty of the gravimetrically prepared mixtures, as listed in table 2. Based on the uncertainty analysis of Schäfer [22] only the percentage uncertainty of the main component of the mixture is calculated. Furthermore, $\Delta\rho$ is the difference between a density calculated with the mixture compositions as given in table 2 and a density calculated with a composition changed by $\Delta x_{\mathrm{CO_2}}$. Thereby, $\Delta x_{\mathrm{CO_2}}$, was of the order of the uncertainty in composition, $u(x_{\mathrm{CO_2}})$ for each mixture as given in table 2. With this method, the relative standard uncertainty, $u[\rho(x_{\mathrm{CO_2}})]/\rho$, caused by the uncertainty in the mixture composition is estimated to be 0.0010 %. This contribution only accounts for the uncertainty of the gravimetrically prepared mixtures. Still, the composition of the gas mixtures in sample cylinders and the composition of the sample in the measuring cell can be different. As reported by Richter and Kleinrahm [20], this is especially valid for measurements in the gas phase of mixtures. To reduce this effect the sample cylinder was rolled to homogenize the mixture before it was attached to the densimeter. In addition, the sample cylinder was constantly heated at its bottom to trigger convection inside the cylinder. Nevertheless, in reproducibility tests performed in this work, small offsets between the different measurement runs could be observed, which were ranging between 0.005 % at high temperatures and up to 0.050 % at low temperatures and high pressures. This is not only caused by the reproducibility of the densimeter itself, but also by sorption effects

in the filling lines and in the measuring cell as well as by the (not entirely) supercritical filling procedure. Accordingly, an extra allowance of $u(\rho_{\mathrm{repro}}) = 0.025\,\%\ \rho_{\mathrm{exp}}$ was added to the uncertainty analysis accounting for these effects. Finally, the standard uncertainty of the density measurement in mixtures, $u_{\mathrm{c}}[\rho(T,p,x)]$, by means of the single-sinker densimeter can be estimated by:

$$u_{\mathrm{c}}[\rho(T,p,x)] = \sqrt{u_{\mathrm{c}}[\rho(T,p)]^2 + u[\rho(x_{\mathrm{CO_2}})]^2 + u(\rho_{\mathrm{repro}})^2}. \tag{8}$$

The uncertainty was calculated for each individual measured (T, p) state point and is listed alongside with the results of the density measurements in tables 5 and 6. Overall, the final estimate for the average relative combined expanded uncertainty ($k = 2$) for the measurements in the 0.50 mole fraction carbon dioxide mixtures ranged from (0.059 to 0.127) % and for the measurements in the 0.75 mole fraction carbon dioxide mixtures from (0.060 to 0.150) %.

3.4 Results and Comparisons to Equations of State

We carried out density measurements on four (argon + carbon dioxide) mixtures with approximately (0.50 and 0.75) mole fraction carbon dioxide over the temperature range of (253.15 to 453.15) K with pressures up to 20 MPa; the phase diagrams of the mixtures and overviews of the measured (p, ρ, T, x) data are given in figures 7 and 9. As listed in table 2, mixture 1a had a composition of 0.50000 mole fraction carbon dioxide—this mixture was only used to carry out the measurements in the gas phase at 253.15 K. Mixture 1b had a composition of 0.49975 mole fraction carbon dioxide and was used for all other isotherms. With mixture 2a (0.75093 mole fraction carbon dioxide) gas-phase measurements [*i.e.*, at T = (253.15, 273.15, and 283.15) K] were performed, and mixture 2b (0.74985 mole fraction carbon dioxide) was used to measure the remaining isotherms. Generally, measurements were carried out at five (T, p) state points along each of five isotherms at T = (253.15, 273.15, 293.15, 353.15, and 453.15) K. However, extensive reproducibility tests in the vicinity of the phase boundary and in the critical region of the 0.50 mole fraction carbon dioxide mixtures [*i.e.*, at T = (253.15 and 273.15) K] led to a total of 51 (p, ρ, T, x) data points for mixtures 1a and 1b; these are all tabulated in table 5. Reproducibility tests with the 0.75 mole fraction carbon dioxide mixtures were only performed in the liquid region at $T = 253.15$ K. However, an additional isotherm at $T = 283.15$ K was measured to increase the overlap area with the data measured by Ben Souissi et al. [7]. Furthermore, in the gas phase of this mixture, flushing points (*i.e.*, a measurement performed after isobaric flushing of the measuring cell, as described above) were carried out, leading to a total of 62 (p, ρ, T, x) data points for mixtures 2a and 2b; the data are listed in table 6. All density values calculated from the equations of state discussed in this work [*i.e.*, the EOS-CG-2021 of Neumann et al. [1] and the GERG-2008 of Kunz and Wagner [3]] were computed with the software package TREND 6.0 [24].

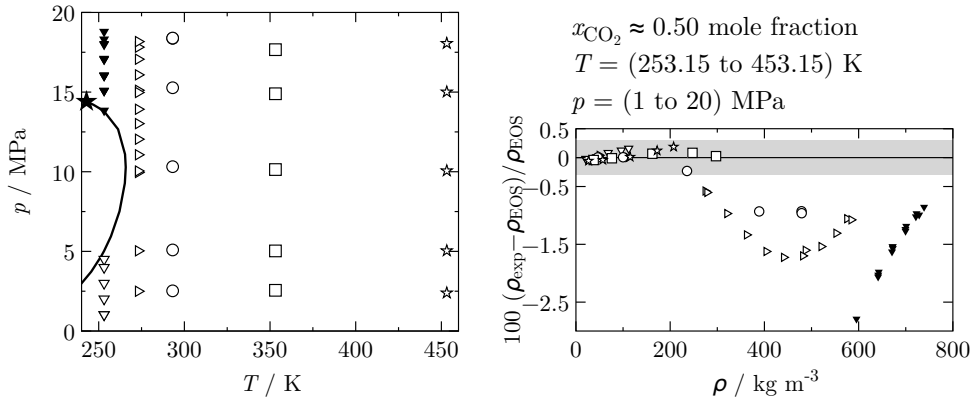


Fig. 7 Results of density measurements on the (0.50 argon + 0.50 carbon dioxide) mixtures. On the left side, the respective (p, T) diagram with the phase boundary is depicted. The phase boundary was calculated with the EOS-CG-2021 of Neumann et al. [1]; ★, critical point; the (p, ρ, T, x) state points measured in the present work are depicted with the same symbols as in the right panel. On the right side, relative deviations of experimental densities, ρ_{exp}, from values, ρ_{EOS}, calculated with the EOS-CG-2021 of Neumann et al. [1] are plotted versus density, ρ. ▽, 253.15 K (gas phase), ▼, 253.15 K (liquid phase), ▷, 273.15 K; ○, 293.15 K; □, 353.15 K; ⋆, 453.15 K. The gray area represents the uncertainty of ±0.3 % stated by Løvseth et al. [8] for homogeneous gas-phase and supercritical densities of the (argon + carbon dioxide) subsystem of the EOS-CG-2021 at pressures up to 30 MPa over most of the composition range; no uncertainty is given for liquid-phase densities.

3.4.1 Results for the Measurements on (0.50 Argon + 0.50 Carbon Dioxide) Mixtures

Figure 7 shows the results of the measurements on the (0.50 argon + 0.50 carbon dioxide) mixtures compared to the EOS-CG-2021 of Neumann et al. [1]. On the left side, the respective (p, T) diagram with the phase boundary is depicted. The phase boundary was calculated with the EOS-CG-2021 of Neumann et al. [1] and all densities measured on the (0.50 argon + 0.50 carbon dioxide) mixtures are shown in this diagram (see circles). On the right side, relative deviations of experimental densities from calculated values are plotted versus density. For the two isotherms at higher temperatures [T = (353.15 and 453.15) K, in figure 7 see squares and stars, respectively] and generally for densities below 200 kg m^{-3}, the equation of state is in good agreement with the measured data. The experimental densities measured at T = 293.15 K (see circles) are still in reasonable agreement with the equation of state, only the data point at approximately 390 kg m^{-3} is not in line with the stated uncertainty of the equation. However, for the isotherms at T = (253.15 and 273.15) K (see down-pointing and right-pointing triangles, respectively) and densities above 200 kg m^{-3}, large deviations compared to the equation can be seen. For the T = 273.15 K isotherm, a characteristic parabolic trend can be observed, which has its maximal negative deviation of −1.73 % at 440 kg m^{-3}, in close proximity to the phase boundary. Richter and McLinden [25] observed a similar behavior compared to the GERG-2008 equation of state by Kunz and Wagner [3] for measurements in the critical region of a (0.74977

methane + 0.25023 propane) mixture utilizing a two-sinker densimeter. For the measurements in the liquid phase at $T = 253.15\,\mathrm{K}$ (see filled down-pointing triangles), this parabolic trend is not closed and large negative deviations can be observed. For this temperature, the relative deviations vs. the EOS-CG-2021 range from (−2.79 to 0.16) %. In summary, only the data points at high temperatures and low densities lie within the uncertainty stated for homogeneous gas-phase and supercritical densities; for liquid-phase densities, no uncertainty is stated (see the caption of figure 7).

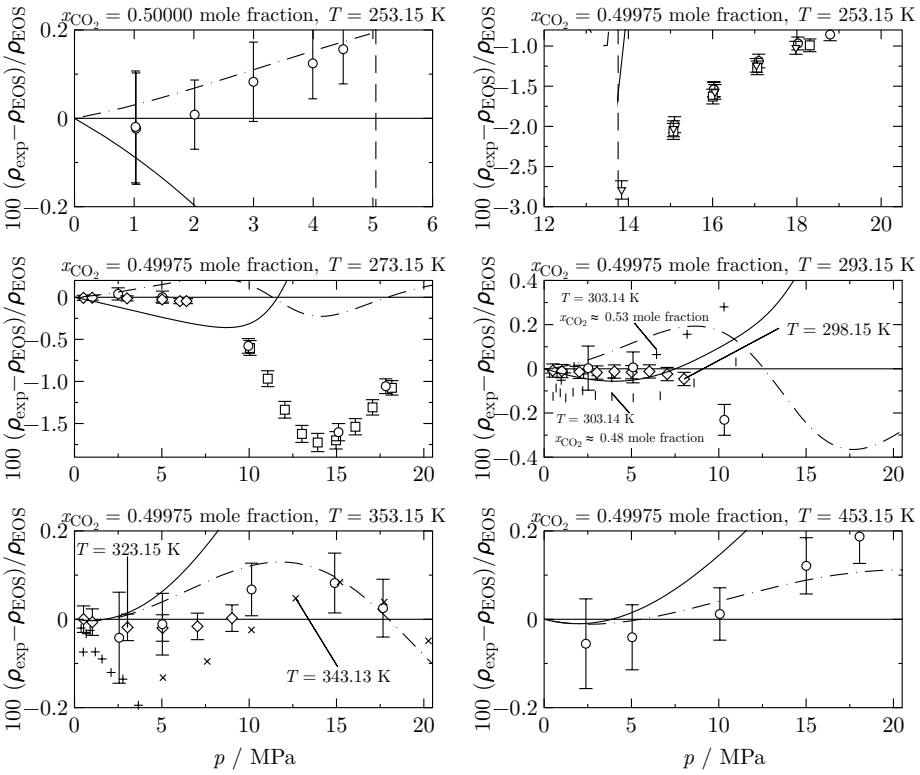


Fig. 8 Results of density measurements on (0.50 argon + 0.50 carbon dioxide) mixtures. Relative deviations of experimental densities, ρ_{exp}, from values, ρ_{EOS}, calculated with the EOS-CG-2021 of Neumann et al. [1] are plotted versus pressure, p. ○, this work (including error bars for (±0.059 to ±0.127) % measurement uncertainty, $k = 2$); □, this work (first repeatability test, including error bars); △, this work (second repeatability test, including error bars); ×, Abraham and Bennett [26]; +, Altunin and Koposhilov [27]; ◇, Ben Souissi et al. [7] (including error bars for ±0.02 % measurement uncertainty, $k = 2$); —, GERG-2008 equation of state by Kunz and Wagner [3]; - · - EOS-CG of Gernert and Span [2]; - -, phase boundary (calculated with the EOS-CG-2021).

In figure 8, relative deviations of the measured densities from values calculated with the EOS-CG-2021 of Neumann et al. [1] are plotted versus pressure. The deviation plots include the data reported by Abraham and Bennett [26, see pluses], Altunin and Koposhilov [27, see crosses], and Ben Souissi et al. [7, see diamonds]. Furthermore, the GERG-2008 equation of state by Kunz and Wagner [3, see solid line] and the

EOS-CG by Gernert and Span [2, see dash-dotted line] are plotted. As already stated above, the EOS-CG-2021 represents the present data well in areas of low densities and at high temperatures. In contrast, at high densities and low temperatures large deviations can be observed. Hence, to improve the clarity of the data visualization, two deviation plots for the lowest temperature (253.15 K) are shown. The measurements carried out in the liquid region at $T = 253.15$ K show the largest deviations compared to the EOS-CG-2021 (up to -2.79 %) of the present measurements. The magnitude of this deviation increases rapidly when approaching the phase boundary. Measurements in very close proximity to the (calculated) phase boundary (see the data point at $p = 13.84$ MPa) have been carried out. Test measurements performed in the course of this work showed that an abrupt change in the magnitude of the deviation can be observed if the mixture inside the measuring cell decomposes into two phases. However, the point at $p = 13.84$ MPa still fits into the pattern of the other data at this particular temperature, hence, we assume that this point is still in the homogeneous region of the mixture. Due to the high deviations compared to the EOS-CG-2021, three replicates (see circles, squares, and triangles in figure 8) were carried out at this temperature, and for all three runs, the above-described supercritical filling procedure was applied. It can be seen that the results for all three measurement runs agree within the uncertainty of the experimental data, thus, we assume that these large deviations may be caused by a limitation of the binary sub-model rather than by errors in our measurements—although an independent confirmation by other laboratories would be desirable.

At $T = (273.15$ and $293.15)$ K, the above-described characteristic parabolic trend can be seen again. For both temperatures the minimum of the parabola is just below 15 MPa. To investigate this slope more precisely, reproducibility measurements were performed at 273.15 K (see squares). For this measurement run, the average step width in pressure of 5 MPa was decreased to 1 MPa. Thereby, deviations of approximately -1.73 % between (14 and 15) MPa could be observed, which corresponds to the critical pressure of the mixture ($p_{\mathrm{crit}} = 14.41$ MPa). At the two higher temperatures [$T = (353.15$ and $453.15)$ K], the EOS-CG-2021 is in good agreement with the new experimental data.

Ben Souissi et al. [7] carried out measurements on (argon + carbon dioxide) mixtures with approximately 0.50 mole fraction carbon dioxide at $T = (273.15$, 298.15, and $323.15)$ K and pressures up to 9 MPa utilizing a two-sinker densimeter. Our data agree within their uncertainty with the densities measured by Ben Souissi et al. [7]. Especially, on the isotherms showing large deviations compared to the EOS-CG-2021 [*i.e.*, $T = (253.15$ and $273.15)$ K] the good agreement of the two data sets in the low density range gives us further confidence to assume, that the observed large deviations in the high density range are due to a limitation of the binary sub-model.

Further experimental data for the (argon + carbon dioxide) system were published by Abraham and Bennett [26], Sarashina et al. [28], Schönmann [29], Kosov and Brovanov [30], Altunin and Koposhilov [27], Altunin and Koposhilov [31], and Mantovani et al. [32] (see Yang et al. [33] for a thorough review of experimental data on carbon-dioxide-rich mixtures). However, most of these measurements were either conducted in different (T, p, x) regions, or the results are off scale in figure 8. Only

the data sets published by Abraham and Bennett [26] and Altunin and Koposhilov [27] can be compared to the new data at $T = (293.15$ and $353.15)$ K, respectively. Thereby, at lower pressures the new experimental data show a reasonable agreement with the data measured by Abraham and Bennett [26]. However, above $p = 8$ MPa the data sets diverge and large deviations can be observed. The measurements published by Altunin and Koposhilov [27] show good agreement with the data measured in this work above $p = 12.5$ MPa. At lower pressures deviations up to 0.1 % can be seen.

The agreement of the densities reported in this work with values calculated from the GERG-2008 equation of state by Kunz and Wagner [3] is over the entire pressure and temperature range not good; deviations between $(-6.51$ to $0.76)$ % can be observed. It should be noted that the GERG-2008 predicts a bubble-point pressure of 14.96 MPa for the 0.49975 mole fraction carbon dioxide mixture at $T = 253.15$ K; the liquid-phase state points measured at lower pressures are thus located within the two-phase region predicted by this equation of state. In this region, calculated homogeneous densities correspond to the metastable liquid root, and the magnitude of the largest deviations therefore also depends on the density-solver implementation used.

The behavior of the EOS-CG of Gernert and Span [2] is included as the dash-dotted line in figure 8. Over the investigated temperature and pressure range, the EOS-CG and the EOS-CG-2021 yield very similar predictions for the (0.50 argon + 0.50 carbon dioxide) mixtures, and accordingly the deviations of the present data from the EOS-CG are comparable in magnitude and trend to those from the EOS-CG-2021. In particular, in the region of low temperatures and high pressures, where the largest deviations are observed, the update from the EOS-CG to the EOS-CG-2021 has not led to a noticeable improvement in the representation of the present data—consistent with the fact that the present data have not been included in the fit of either model (see introduction).

Table 5: Experimental (p, ρ, T, x) data for the (0.50 argon + 0.50 carbon dioxide) mixtures (all replicates are listed), relative deviations of the experimental data, ρ_{exp}, from densities, ρ_{EOS}, calculated with the EOS-CG-2021 of Neumann et al. [1], and the combined expanded uncertainty, U_{c} ($k = 2$), of the density measurements are listed. p is the pressure and T is the temperature (ITS-90). The expanded uncertainty ($k = 2$) in temperature, $U(T)$, was 17 mK and the expanded uncertainty ($k = 2$) in pressure, $U(p)$, was 4.0 hPa for 0.5 MPa $< p <$ 2.5 MPa, 15.9 hPa for 2.5 MPa $< p <$ 12.0 MPa, and 47.8 hPa for $p >$ 12.0 MPa.

p / MPa	T / K	ρ_{exp} / kg m^{-3}	$100\frac{(\rho_{\mathrm{exp}}-\rho_{\mathrm{EOS}})}{\rho_{\mathrm{EOS}}}$	$\frac{U_{\mathrm{c}}(\rho)}{\rho}$ / %
0.49975 mole fraction carbon dioxide				
18.78894	253.150	738.8608	−0.8567	0.0772
18.02525	253.150	722.8835	−0.9681	0.0803
17.09541	253.150	700.9745	−1.1862	0.0848
16.03161	253.149	672.1755	−1.5399	0.0916
16.02783	253.151	672.0553	−1.5403	0.0919
15.09519	253.150	642.6616	−1.9791	0.0995

continued on next page

Table 5 (continued)

p / MPa	T / K	ρ_{exp} / kg m^{-3}	$100\frac{(\rho_{exp}-\rho_{EOS})}{\rho_{EOS}}$	$\frac{U_c(\rho)}{\rho}$ / %
0.49975 mole fraction carbon dioxide; first repeatability test				
18.30668	253.145	728.4855	−0.9910	0.0791
17.05891	253.148	699.5386	−1.2716	0.0851
16.00427	253.150	670.8310	−1.6292	0.0919
15.06974	253.149	641.3483	−2.0629	0.0998
0.49975 mole fraction carbon dioxide; second repeatability test				
17.97621	253.150	721.4743	−1.0217	0.0805
17.04060	253.150	699.3187	−1.2404	0.0852
16.05340	253.150	672.5309	−1.5711	0.0915
15.07073	253.150	641.5836	−2.0302	0.0997
13.83962	253.151	595.4358	−2.7917	0.1142
0.50000 mole fraction carbon dioxide				
4.50264	253.150	111.9842	0.1565	0.0786
3.99242	253.151	96.2698	0.1244	0.0802
2.99735	253.151	68.4089	0.0827	0.0898
2.01336	253.151	43.7491	0.0084	0.0783
1.03102	253.152	21.4375	−0.0233	0.1260
1.02256	253.153	21.2547	−0.0194	0.1266
0.49975 mole fraction carbon dioxide				
17.81995	273.144	575.4128	−1.0565	0.0875
15.11480	273.151	487.3867	−1.6028	0.1021
9.95410	273.149	274.8132	−0.5779	0.0869
5.03462	273.150	111.1100	0.0015	0.0721
2.49724	273.150	50.0780	0.0398	0.0726
0.49975 mole fraction carbon dioxide; first repeatability test				
18.16998	273.155	584.5750	−1.0762	0.0860
17.06385	273.147	552.5807	−1.3080	0.0913
16.08204	273.151	520.9048	−1.5385	0.0966
14.97406	273.150	481.8059	−1.6997	0.1031
13.92265	273.149	441.2770	−1.7257	0.1084
13.02003	273.150	404.1649	−1.6235	0.1011
12.04217	273.150	362.6415	−1.3365	0.0992
11.06459	273.150	320.8691	−0.9675	0.0943
10.04598	273.150	278.5365	−0.6024	0.0876
0.49975 mole fraction carbon dioxide				
18.39122	293.149	479.1306	−0.9616	0.0810
18.37375	293.148	478.8361	−0.9279	0.0853
15.27252	293.151	388.9414	−0.9309	0.0866
10.31782	293.150	235.7421	−0.2310	0.0698
5.08974	293.150	100.0325	0.0064	0.0700
2.52228	293.150	46.2492	0.0031	0.0999
0.49975 mole fraction carbon dioxide				
17.66320	353.149	297.3246	0.0252	0.0654
14.89593	353.151	247.3832	0.0821	0.0677
10.13737	353.149	162.1833	0.0675	0.0595

continued on next page

Table 5 (continued)

p / MPa	T / K	ρ_{exp} / kg m^{-3}	$100\frac{(\rho_{\mathrm{exp}}-\rho_{\mathrm{EOS}})}{\rho_{\mathrm{EOS}}}$	$\frac{U_{\mathrm{c}}(\rho)}{\rho}$ / %
5.02921	353.149	76.2602	−0.0111	0.0698
2.55600	353.152	37.6580	−0.0417	0.1030
0.49975 mole fraction carbon dioxide				
18.05875	453.147	207.3159	0.1873	0.0609
15.00873	453.150	172.3804	0.1210	0.0637
10.06061	453.150	115.0511	0.0120	0.0593
5.04053	453.151	57.0511	−0.0407	0.0736
2.39153	453.151	26.8559	−0.0553	0.1015

3.4.2 Results for the Measurements on (0.25 Argon + 0.75 Carbon Dioxide) Mixtures

On the left side of figure 9, the respective (p, T) diagram of the (0.25 argon + 0.75 carbon dioxide) mixtures with the phase boundary is depicted. The phase boundary was calculated with the EOS-CG-2021 of Neumann et al. [1] and all densities measured on these mixtures are shown in this diagram (see circles). On the right side, relative deviations of experimental densities ρ_{exp} from values ρ_{EOS} calculated with the EOS-CG-2021 of Neumann et al. [1] are plotted versus density ρ. The data points at low densities and high temperatures show the best agreement with the EOS-CG-2021. Again, the largest deviations can be observed at high densities and low temperatures (*i.e.* $T = 253.15\,\mathrm{K}$, see filled down-pointing triangles in figure 9). However, the measurements performed in the liquid phase at $T = 273.15\,\mathrm{K}$ are in very good agreement with the EOS-CG-2021. The data measured at $T = 293.15\,\mathrm{K}$ also show a parabolic deviation trend, with a maximum deviation of 0.69 % at $700\,\mathrm{kg\,m^{-3}}$. This pattern may be retrieved in the deviations at $T = (253.15,\ 273.15,\ \mathrm{and}\ 353.15)\,\mathrm{K}$, for the data points measured above the phase boundary. Overall, the relative deviations compared to the EOS-CG-2021 range from (−0.53 to 0.69) %.

Relative deviations of the measured densities from values calculated with the EOS-CG-2021 of Neumann et al. [1] are plotted versus pressure in figure 10. Experimental densities reported by Abraham and Bennett [26, see crosses], Altunin and Koposhilov [27, see pluses], and Ben Souissi et al. [7, see diamonds] are included in the plots. Furthermore, the behavior of the GERG-2008 equation of state by Kunz and Wagner [3, solid line] and of the EOS-CG by Gernert and Span [2, dash-dotted line] are also presented in the deviation plots. The measurements in the gas phase and in the liquid phase along the isotherms at $T = (253.15\ \mathrm{and}\ 273.15)\,\mathrm{K}$ were carried out with different mixtures, hence, the results are depicted in individual deviation plots. Generally, the deviations from the EOS-CG-2021 are substantially smaller than for the 0.50 mole fraction carbon dioxide mixtures. Only in the liquid region at $T = 253.15\,\mathrm{K}$ somewhat larger deviations can be observed, which increase to −0.53 % when approaching the phase boundary. The two data points in the vicinity of the phase boundary may be considered as outliers. As above-described, an abrupt change in the magnitude of the deviation indicates that the mixture in the measuring cell has decomposed into two phases. Hence, it is likely that at $p = 12\,\mathrm{MPa}$ a gas phase is already present. To confirm the large deviations compared to the EOS-CG-2021, a reproducibility test (see

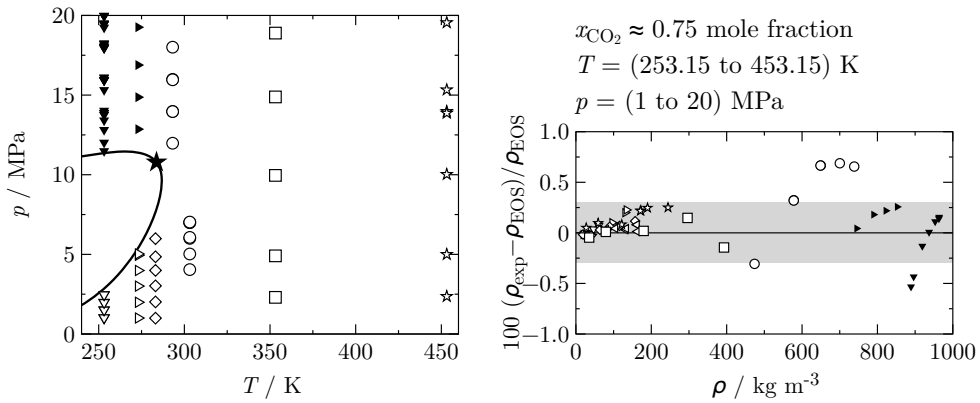


Fig. 9 Results of density measurements on the (0.25 argon + 0.75 carbon dioxide) mixtures. On the left side, the respective (p, T) diagram with the phase boundary is depicted. The phase boundary was calculated with the EOS-CG-2021 of Neumann et al. [1]; ★, critical point; the (p, ρ, T, x) state points measured in the present work are depicted with the same symbols as in the right panel. On the right side, relative deviations of experimental densities, ρ_{exp}, from values, ρ_{EOS}, calculated with the EOS-CG-2021 of Neumann et al. [1] are plotted versus density, ρ. ▽, 253.15 K (gas phase), ▼, 253.15 K (liquid phase), ▷, 273.15 K (gas phase); ▶, 273.15 K (liquid phase); ◇, 283.15 K; ○, 293.15 K; □, 353.15 K; ⋆, 453.15 K. The gray area represents the uncertainty of ±0.3 % stated by Løvseth et al. [8] for homogeneous gas-phase and supercritical densities of the (argon + carbon dioxide) subsystem of the EOS-CG-2021 at pressures up to 30 MPa over most of the composition range; no uncertainty is given for liquid-phase densities.

rectangles) was carried out. Both measurement runs agree within the uncertainty of the measured data, although a comparably large deviation between the two series of measurements can be observed (up to 0.05 % for single data points). These deviations are likely caused by the not entirely supercritical filling procedure. Hence, for future measurements in such mixtures, we will further enhance the apparatus to enable a fully supercritical filling of the measuring cell at low temperatures. The measurements carried out at $T = 293.15$ K proved to be rather complicated. Due to the close proximity to the critical region, density fluctuations in the measuring cell yielded very unstable balance readings. However, the obtained results show large positive deviations of 0.69 %, which decrease rapidly when approaching the critical region (down to −0.31 %). For the other isotherms, the deviations mostly range between (−0.1 to 0.1) %. However, single data points, *e.g.*, in the vicinity of the phase boundary at $T = 273.15$ K, show larger deviations.

As already stated above, flushing points have been carried out in the gas phase (see filled circles in figure 10). It can be seen that the deviations between 'normal' measuring points (unfilled circles) and the flushing points are mostly small and always within the uncertainty of the present measurements. It is very unlikely that sorption effects are weak in the investigated mixture. Rather, this illustrates again that the design of the measuring cell does not allow proper flushing—even at low densities. Accordingly, to save sample fluid, isobaric flushing of the measuring cell was not performed for any other measurements in the gas phase. In the course of this work, purging points (*i.e.*, venting the sample and re-pressurizing the measuring cell to the

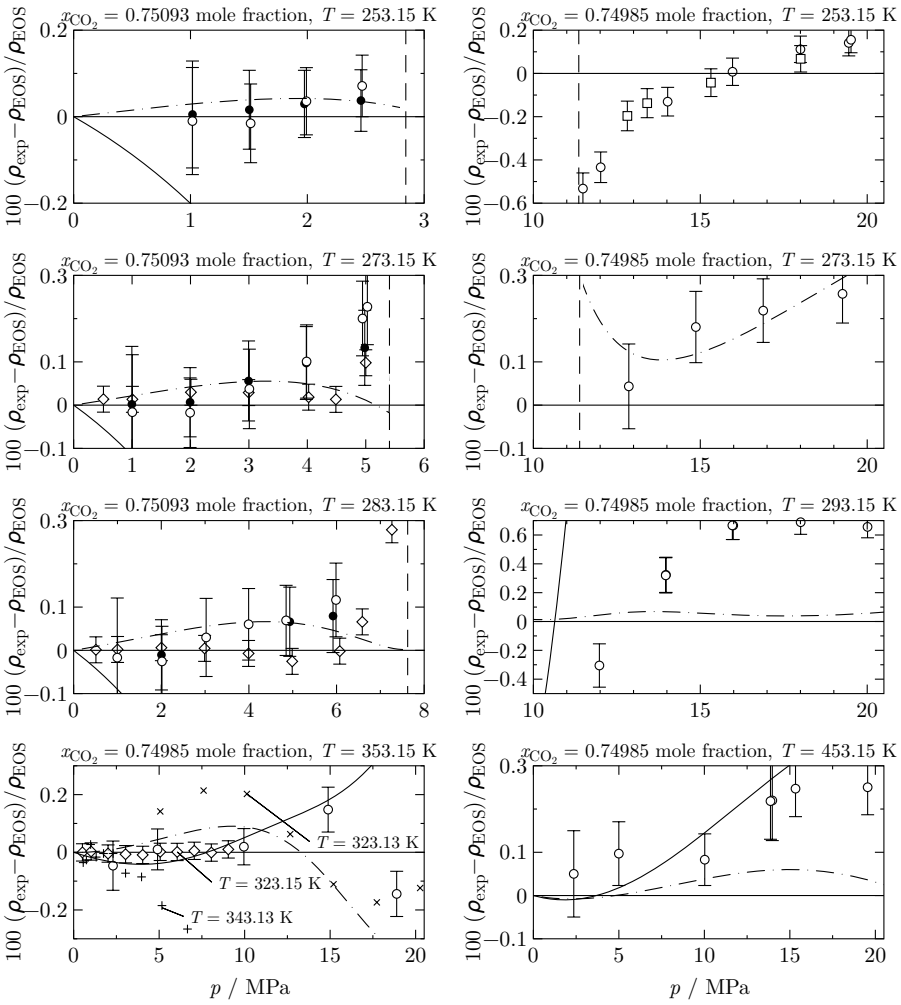


Fig. 10 Results of density measurements on (0.25 argon + 0.75 carbon dioxide) mixtures. Relative deviations of experimental densities, ρ_{exp}, from values, ρ_{EOS}, calculated with the EOS-CG-2021 of Neumann et al. [1] are plotted versus pressure, p. ○, this work (including error bars for (±0.060 to ±0.150) % measurement uncertainty, k = 2); ●, this work (flushing points, including error bars); □, this work (repeatability test, including error bars); ×, Abraham and Bennett [26]; +, Altunin and Koposhilov [27]; ◇, Ben Souissi et al. [7, including error bars for ±0.02 % measurement uncertainty, k = 2]; —, GERG-2008 equation of state by Kunz and Wagner [3]; - · - EOS-CG of Gernert and Span [2]; - -, phase boundary (calculated with the EOS-CG-2021).

desired pressure) were not tested. Due to the high densities of the (argon + carbon dioxide) mixtures in the investigated (T, p) range, this procedure would have required too large an amount of the available mixtures.

Ben Souissi et al. [7] also carried out density measurements on an (0.25155 argon + 0.74845 carbon dioxide) mixture at T = (273.15, 283.15, 293.15, and 323.15) K and with pressures up to 9 MPa utilizing a two-sinker densimeter (see diamonds in figure

10). Again, the present data agree well with the densities measured by Ben Souissi et al. [7].

The agreement with the data set reported by Abraham and Bennett [26] is not good. Deviations of up to 0.2 % can be observed. At pressures below 2.5 MPa the new experimental data agree within the uncertainty of the present measurements with the results reported by Altunin and Koposhilov [27]. However, above that pressure large deviations can be observed and the densities reported by Altunin and Koposhilov [27] are off scale above $p = 5$ MPa.

The behavior of the GERG-2008 equation of state does not really agree with the presently measured densities; the relative deviations range between (−4.24 to 1.68) %. At $T = 353.15$ K the experimental densities measured in this work and the data measured by Ben Souissi et al. [7] seem to agree better with the GERG-2008 than with the EOS-CG-2021. However, the sharp increase of the slope of the GERG-2008 above 10 MPa does not agree with the experimental results at $p = 20$ MPa.

The EOS-CG of Gernert and Span [2] is included as the dash-dotted line in figure 10. For the 0.75 mole fraction carbon dioxide mixtures, the deviations of the present data from the EOS-CG are similar in magnitude and trend to those from the EOS-CG-2021. In particular, in the region of low temperatures and high pressures, the update from the EOS-CG to the EOS-CG-2021 has not led to a noticeable improvement in the representation of the present data, suggesting that the remaining deviations may originate from limitations of the binary sub-model in a region that is still weakly constrained by experimental information (see introduction).

Table 6: Experimental (p, ρ, T, x) data for the (0.25 argon + 0.75 carbon dioxide) mixtures (all replicates are listed), relative deviations of the experimental data, ρ_{exp}, from densities, ρ_{EOS}, calculated with the EOS-CG-2021 of Neumann et al. [1], and the combined expanded uncertainty, U_{c} ($k = 2$), of the density measurements are listed. p is the pressure and T is the temperature (ITS-90). The expanded uncertainty ($k = 2$) in temperature, $U(T)$, was 17 mK and the expanded uncertainty ($k = 2$) in pressure, $U(p)$, was 4.0 hPa for 0.5 MPa $< p <$ 2.5 MPa, 15.9 hPa for 2.5 MPa $< p <$ 12.0 MPa, and 47.8 hPa for $p >$ 12.0 MPa.

p / MPa	T / K	ρ_{exp} / kg m^{-3}	$100\frac{(\rho_{\mathrm{exp}}-\rho_{\mathrm{EOS}})}{\rho_{\mathrm{EOS}}}$	$\frac{U_{\mathrm{c}}(\rho)}{\rho}$ / %
0.74985 mole fraction carbon dioxide				
19.51497	253.149	963.7365	0.1556	0.0599
19.44734	253.151	963.1511	0.1412	0.0601
17.99960	253.152	953.1168	0.1116	0.0611
15.96600	253.151	936.9729	0.0077	0.0632
14.02228	253.151	919.0761	−0.1306	0.0662
12.01605	253.150	896.0883	−0.4339	0.0707
11.48416	253.151	889.1152	−0.5325	0.0724
0.74985 mole fraction carbon dioxide; repeatability test				
18.00612	253.153	952.7383	0.0676	0.0611
15.31803	253.151	931.2274	−0.0427	0.0641

continued on next page

Table 6 (continued)

p / MPa	T / K	ρ_{exp} / kg m^{-3}	$100\frac{(\rho_{\mathrm{exp}}-\rho_{\mathrm{EOS}})}{\rho_{\mathrm{EOS}}}$	$\frac{U_{\mathrm{c}}(\rho)}{\rho}$ / %
13.40918	253.152	913.2103	−0.1375	0.0672
12.81514	253.149	906.7643	−0.1966	0.0685
0.75093 mole fraction carbon dioxide				
2.46922	253.148	60.7107	0.0711	0.0712
1.99212	253.151	46.8818	0.0357	0.0777
1.51470	253.151	34.2698	−0.0154	0.0910
1.01640	253.150	22.1682	−0.0101	0.1238
0.75093 mole fraction carbon dioxide; flushing points				
2.45885	253.152	60.3731	0.0373	0.0712
1.97513	253.153	46.4109	0.0295	0.0777
1.50343	253.152	33.9957	0.0160	0.0912
1.01712	253.151	22.1883	0.0051	0.1236
0.74985 mole fraction carbon dioxide				
19.26048	273.148	852.5754	0.2573	0.0675
16.88461	273.151	822.5231	0.2185	0.0735
14.86675	273.151	789.8758	0.1806	0.0824
12.85873	273.150	745.0172	0.0434	0.0980
0.75093 mole fraction carbon dioxide				
5.02767	273.148	134.3488	0.2274	0.0876
4.94464	273.138	130.9451	0.2003	0.0863
3.98735	273.152	96.4259	0.1009	0.0847
3.00737	273.151	67.4533	0.0375	0.0919
1.99319	273.150	41.8682	−0.0175	0.0805
1.00411	273.151	19.9661	−0.0163	0.1329
0.75093 mole fraction carbon dioxide; flushing points				
4.98276	273.148	132.3843	0.1325	0.0868
3.98236	273.150	96.2632	0.0974	0.0842
2.99406	273.143	67.1085	0.0559	0.0925
1.99338	273.151	41.8826	0.0067	0.0800
0.99644	273.150	19.8094	0.0019	0.1339
0.75093 mole fraction carbon dioxide				
5.98766	283.150	157.1975	0.1165	0.0852
5.91986	283.150	154.3766	0.0793	0.0844
4.93260	283.152	118.3341	0.0661	0.0800
4.84904	283.151	115.5958	0.0692	0.0811
3.99348	283.151	89.6223	0.0602	0.0827
3.02352	283.151	63.9157	0.0298	0.0903
2.00381	283.152	40.0835	−0.0104	0.0812
2.01568	283.152	40.3390	−0.0256	0.0812
0.99534	283.150	18.9726	−0.0169	0.1379
0.74985 mole fraction carbon dioxide				
20.00975	293.149	738.4517	0.6563	0.0757
18.00635	293.150	700.1879	0.6887	0.0840
15.96037	293.151	648.9042	0.6666	0.0980
15.98653	293.149	649.6757	0.6663	0.0977

continued on next page

Table 6 (continued)

p / MPa	T / K	ρ_{exp} / kg m^{-3}	$100\frac{(\rho_{\mathrm{exp}}-\rho_{\mathrm{EOS}})}{\rho_{\mathrm{EOS}}}$	$\frac{U_{\mathrm{c}}(\rho)}{\rho}$ / %
13.96489	293.148	577.9110	0.3200	0.1222
13.97092	293.151	578.1517	0.3237	0.1220
11.97732	293.151	473.9927	−0.3052	0.1503
0.74985 mole fraction carbon dioxide				
18.89152	353.151	392.9527	−0.1443	0.0784
14.88371	353.142	296.2153	0.1480	0.0778
9.95697	353.152	179.6966	0.0193	0.0629
4.90694	353.155	79.3680	0.0100	0.0709
2.30074	353.152	35.2361	−0.0464	0.0854
0.74985 mole fraction carbon dioxide				
19.54896	453.148	244.4245	0.2504	0.0636
15.33062	453.152	190.0541	0.2471	0.0647
13.97309	453.154	172.4527	0.2198	0.0927
13.86681	453.153	171.0780	0.2183	0.0882
10.02242	453.150	121.5790	0.0829	0.0597
4.99745	453.152	59.0055	0.0969	0.0737
2.36208	453.150	27.4114	0.0501	0.0998

4 Summary

We presented accurate (p, ρ, T, x) data, measured over the temperature range from (253.15 to 453.15) K with pressures up to 20 MPa utilizing a single-sinker densimeter. Four mixtures were investigated to cover a large part of the temperature and pressure range of the (argon + carbon dioxide) system with approximately (0.50 and 0.75) mole fraction carbon dioxide. The average relative combined expanded uncertainty ($k = 2$) for the measurements in the 0.50 mole fraction carbon dioxide mixtures was estimated to range from (0.059 to 0.127) % and for the measurements in the 0.75 mole fraction carbon dioxide mixtures to range from (0.060 to 0.150) %.

At low temperatures and high pressures (*i.e.*, in the liquid region of the mixtures) the first results of the measurements showed large, non-reproducible deviations from the EOS-CG-2021 of Neumann et al. [1]. We assumed that these deviations arose from a decomposition of the mixture during the pressurization of the measuring cell. Hence, a supercritical filling procedure was established. The apparatus was filled gradually, starting with the abrupt pressurization of the sample manifold—assuming that the sample would not have enough time to equilibrate at low pressures and, hence, would not decompose by forming liquid.

A further result of our measurements is that isobaric flushing of the measuring cell (as proposed by Richter and Kleinrahm [20]) is not effective for our device. Both the sample fluid inlet and outlet ports are located in the bottom flange of the measuring cell, directly underneath the sinker. Additionally, the gap between the inner surface of the measuring cell and the outer diameter of the sinker is small. Hence, the volume above the sinker constitutes a dead-end volume that is not traversed by the flow and can only be exchanged slowly through the narrow gap. Even at gas densities the effect of flushing the measuring cell on the results of the density measurements was small,

whereby it is unlikely that sorption effects (in particular close to the phase boundary) are weak in the investigated mixtures. Rather, this confirms the assumption that major proportions of the sample fluid in the measuring cell are not exchanged in the flushing process.

We compared the presented experimental density data for the (argon + carbon dioxide) mixtures to data sets measured by Abraham and Bennett [26], by Altunin and Koposhilov [27], and by Ben Souissi et al. [7]. Additionally, we compared our data to the equations of state by Neumann et al. [1, EOS-CG-2021], by Gernert and Span [2, EOS-CG], and by Kunz and Wagner [3, GERG-2008]. Thereby, especially the agreement with the data reported by Ben Souissi et al. [7] was good. The present data agree with the more accurate data reported by Ben Souissi et al. [7] within the uncertainty of the present measurements. For the 0.50 mole fraction carbon dioxide mixtures, the results obtained in this work were only at high temperatures and low densities within the uncertainty of the EOS-CG-2021. At low temperatures and high densities, large deviations from the equation could be observed (up to −2.79 %). Several reproducibility tests verified this result so that these deviations may be caused by a limitation of the binary sub-model; however, independent confirmation through further measurements would support the conclusions drawn from the present measurements. At $T =$ (273.15 and 293.15) K a characteristic, parabolic trend of the deviations could be seen and the minimum of the parabola was correlated to the critical pressure of the mixture. For the 0.75 mole fraction carbon dioxide mixtures, the deviations from the EOS-CG-2021 were much smaller. The best agreement was again observed at high temperatures and low densities, while at low temperatures and high densities the deviations were somewhat larger (up to −0.53 %). Overall, the relative deviations from the EOS-CG-2021 range from (−2.79 to 0.19) % for the 0.50 mole fraction carbon dioxide mixtures and from (−0.53 to 0.69) % for the 0.75 mole fraction carbon dioxide mixtures.

The agreement of the present experimental densities with the GERG-2008 equation of state of Kunz and Wagner [3] was over the entire pressure and temperature range not good. For the 0.50 mole fraction carbon dioxide mixtures the deviations range between (−6.51 to 0.76) % and for the 0.75 mole fraction carbon dioxide mixtures from (−4.24 to 1.68) %.

The EOS-CG-2021 of Neumann et al. [1] does not represent the present data substantially better than the EOS-CG of Gernert and Span [2]; the deviations of the experimental densities from both equations of state are similar in magnitude and trend, particularly in the region of low temperatures and high pressures. As discussed in the introduction, the present data were not used in the fit of either model. The pronounced trend of the deviations was nevertheless verified in several reproducibility tests, and we consider it likely that the remaining deviations originate from limitations of the binary sub-model rather than from inaccuracies of the present measurements.

Acknowledgements. Robin Wegge is especially grateful for the active support in the laboratory by his student co-workers Tim Wenig, Christian Scholz, and Alexander Maurer. Furthermore, the authors thank Reiner Kleinrahm and Mark McLinden for the fruitful discussions regarding the experimental procedures with a special focus on handling of gas mixtures. Finally, we thank Stefan Herrig and Tobias Neumann for

the insight into the fitting procedures of their new equation of state for the (argon + carbon dioxide) system and their willingness for open discussions.

Statements and Declarations

- **Funding:** The work was supported by the research programme CLIMIT and the BIGCCS Centre, performed under the Norwegian research programme Centres for Environment-friendly Energy Research (FME). We acknowledge the following partners for their contributions: Gassco, Shell, Equinor (formerly Statoil), TotalEnergies, Engie, and the Research Council of Norway (193816/S60 and 200005/S60).
- **Competing Interests:** The authors declare no competing interests.
- **Data availability:** All experimental data are provided in tables within this article.
- **Author contribution:** Robin Wegge designed and carried out the density measurements on (argon + carbon dioxide) mixtures, performed the data evaluation and uncertainty analysis, prepared the figures, and drafted the manuscript. Markus Richter co-developed the experimental concept for purging and supercritical filling of the measuring cell at low temperatures, supervised the experimental work, contributed to the assessment of the results, and revised the manuscript. Roland Span acquired the funding for the third-party project within which this work was carried out, oversaw the project, and revised the manuscript. All authors approved the final version of the manuscript and agree to be accountable for the work.

References

[1] Neumann, T., Herrig, S., Bell, I.H., Beckmüller, R., Lemmon, E.W., Thol, M., Span, R.: EOS-CG-2021: A mixture model for the calculation of thermodynamic properties of CCS mixtures. International Journal of Thermophysics **44**(12), 178 (2023) https://doi.org/10.1007/s10765-023-03263-6

[2] Gernert, G.J., Span, R.: EOS-CG: A Helmholtz Energy Mixture Model for Humid Gases and CCS Mixtures. The Journal of Chemical Thermodynamics **93**, 274–293 (2016) https://doi.org/10.1016/j.jct.2015.05.015

[3] Kunz, O., Wagner, W.: The GERG-2008 Wide-Range Equation of State for Natural Gases and Other Mixtures: An Expansion of GERG-2004. Journal of Chemical & Engineering Data **57**(11), 3032–3091 (2012) https://doi.org/10.1021/je300655b

[4] Gernert, G.J.: A new Helmholtz Energy Model for Humid Gases and CCS Mixtures. PhD thesis, Lehrstuhl für Thermodynamik, Ruhr-Universität Bochum (2013)

[5] Wegge, R., McLinden, M.O., Perkins, R.A., Richter, M., Span, R.: Speed-of-Sound Measurements in (Argon + Carbon Dioxide) Over the Temperature Range From (275 to 500) K at Pressures up to 8 MPa. The Journal of Chemical Thermodynamics **99**, 54–64 (2016) https://doi.org/10.1016/j.jct.2016.03.036

[6] Yang, X., Richter, M., Ben Souissi, M.A., Kleinrahm, R., Span, R.: Vapor-Phase (p, ρ, T, x) Behavior and Virial Coefficients for the Binary Mixture (0.05 Argon + 0.95 Carbon Dioxide) over the Temperature Range from (273.15 to 323.15) K with Pressures up to 9 MPa. Journal of Chemical & Engineering Data **61**(8), 2676–2681 (2016) https://doi.org/10.1021/acs.jced.6b00120

[7] Ben Souissi, M.A., Richter, M., Yang, X., Kleinrahm, R., Span, R.: Vapor-Phase (p, ρ, T, x) Behavior and Virial Coefficients for the (Argon + Carbon Dioxide) System. Journal of Chemical & Engineering Data **62**(1), 362–369 (2017) https://doi.org/10.1021/acs.jced.6b00687

[8] Løvseth, S.W., Austegard, A., Westman, S.F., Stang, H.G.J., Herrig, S., Neumann, T., Span, R.: Thermodynamics of the Carbon Dioxide Plus Argon (CO_2 + Ar) System: An Improved Reference Mixture Model and Measurements of Vapor-Liquid, Vapor-Solid, Liquid-Solid and Vapor-Liquid-Solid Phase Equilibrium Data at the Temperatures (213 to 299) K and Pressures up to 16 MPa. Fluid Phase Equilibria **466**, 48–78 (2018) https://doi.org/10.1016/j.fluid.2018.02.009

[9] Gedanitz, H.: Schallgeschwindigkeits- und Dichtemessungen in Fluiden. PhD thesis, Lehrstuhl für Thermodynamik, Ruhr-Universität Bochum (2010). https://hss-opus.ub.ruhr-uni-bochum.de/opus4/frontdoor/deliver/index/docId/2374/file/diss.pdf

[10] Blahut, A., Prokopová, O., Vinš, V., Štejfa, V., Soba, L., Thol, M., Span, R.: Density, Heat Capacity, and Vapor Pressure of Squalane. International Journal of Thermophysics **47**(2), 25 (2026) https://doi.org/10.1007/s10765-025-03684-5

[11] Wegge, R.: Thermodynamic Properties of the (Argon + Carbon Dioxide) System: Instrument Development and Measurements of Density and Speed of Sound. PhD thesis, Lehrstuhl für Thermodynamik, Ruhr-Universität Bochum (2016). https://hss-opus.ub.ruhr-uni-bochum.de/opus4/frontdoor/deliver/index/docId/4542/file/diss.pdf

[12] Wagner, W., Kleinrahm, R.: Densimeters for Very Accurate Density Measurements of Fluids Over Large Ranges of Temperature, Pressure, and Density. Metrologia **41**(2), 24–39 (2004) https://doi.org/10.1088/0026-1394/41/2/S03

[13] McLinden, M.O.: Chapter 2 — Experimental Techniques 1 (Direct Methods). In: Wilhelm, E., Letcher, T.M. (eds.) Volume Properties: Liquids, Solutions and Vapours. Royal Society of Chemistry, Cambridge, UK (2014)

[14] Richter, M., Kleinrahm, R., Lentner, R., Span, R.: Development of a Special Single-Sinker Densimeter for Cryogenic Liquid Mixtures and First Results for a Liquefied Natural Gas (LNG). The Journal of Chemical Thermodynamics **93**, 205–221 (2016) https://doi.org/10.1016/j.jct.2015.09.034

[15] Kleinrahm, R., Yang, X., McLinden, M.O., Richter, M.: Analysis of the Systematic Force-Transmission Error of the Magnetic-Suspension Coupling in Single-Sinker Densimeters and Commercial Gravimetric Sorption Analyzers. Adsorption **25**(4), 717–735 (2019) https://doi.org/10.1007/s10450-019-00071-z

[16] Yang, X., Kleinrahm, R., McLinden, M.O., Richter, M.: The Magnetic Suspension Balance: 40 Years of Advancing Densimetry and Sorption Science. International Journal of Thermophysics **44**(11), 169 (2023) https://doi.org/10.1007/s10765-023-03269-0

[17] Physikalisch-Technische Bundesanstalt: Kalibrierschein für den Silicium-Senkkörper. Kalibrierzeichen 33.33-208A055, Braunschweig, Germany (2008)

[18] McLinden, M.O., Kleinrahm, R., Wagner, W.: Force Transmission Errors in Magnetic Suspension Densimeters. International Journal of Thermophysics **28**(2), 429–448 (2007) https://doi.org/10.1007/s10765-007-0176-0

[19] Physikalisch-Technische Bundesanstalt: Kalibrierschein für das 25 Ω-Platinwiderstandsthermometer Rosemount 162D. Kalibrierzeichen 37411, Berlin, Germany (1992)

[20] Richter, M., Kleinrahm, R.: Influence of Adsorption and Desorption on Accurate Density Measurements of Gas Mixtures. The Journal of Chemical Thermodynamics **74**, 58–66 (2014) https://doi.org/10.1016/j.jct.2014.03.020

[21] ISO/IEC Guide 98-3: Uncertainty of Measurement – Part 3: Guide to the Expression of Uncertainty in Measurement (GUM:1995). International Organization for Standardization, Geneva, Switzerland (2008)

[22] Schäfer, M.: Improvements to Two Viscometers Based on a Magnetic Suspension Coupling and Measurements on Carbon Dioxide. PhD thesis, Lehrstuhl für Thermodynamik, Ruhr-Universität Bochum (2015). https://hss-opus.ub.ruhr-uni-bochum.de/opus4/frontdoor/deliver/index/docId/4716/file/diss.pdf

[23] Span, R., Lemmon, E.W., Jacobsen, R.T., Wagner, W., Yokozeki, A.: A Reference Equation of State for the Thermodynamic Properties of Nitrogen for Temperatures from 63.151 to 1000 K and Pressures to 2200 MPa. Journal of Physical and Chemical Reference Data **29**(6), 1361–1433 (2000) https://doi.org/10.1063/1.1349047

[24] Span, R., Beckmüller, R., Buchenfeld, J., Fiedler, F., Jäger, A., Mickoleit, E., Neumann, T., Nguyen, T.-T.-G., Pohl, S.M., Rath, S., Sabozin, F., Semrau, B., Thol, M.: TREND. Thermodynamic Reference and Engineering Data 6.0. Lehrstuhl für Thermodynamik, Ruhr-Universität Bochum, Bochum, Germany (2025)

[25] Richter, M., McLinden, M.O.: Vapor-Phase (p, ρ, T, x) Behavior and Virial Coefficients for the (Methane + Propane) System. Journal of Chemical & Engineering

Data **59**(12), 4151–4164 (2014) https://doi.org/10.1021/je500792x

[26] Abraham, W.H., Bennett, C.O.: The Compressibility of Carbon Dioxide-Argon Mixtures. American Institute of Chemical Engineers Journal **6**(2), 257–261 (1960) https://doi.org/10.1002/aic.690060218

[27] Altunin, V.V., Koposhilov, O.D.: Thermal Properties of Gaseous Mixtures of Carbon Dioxide-Argon at Elevated Temperatures. Trudy Moskovskogo Energeticheskogo Instituta [in Russian] **313**, 20–23 (1976)

[28] Sarashina, E., Arai, Y., Sasto, S.: The PVTX Relation for the Carbon Dioxide-Argon System. Journal of Chemical Engineering of Japan **4**(4), 379–381 (1971) https://doi.org/10.1252/jcej.4.379

[29] Schönmann, W.: Messung der thermischen eigenschaften und aufstellung einer empirischen zustandsgleichung gasförmiger argon-kohlendioxid-gemische. PhD thesis, Fakultät für Chemieingenieurwesen, Universität Karlsruhe (1971)

[30] Kosov, N.D., Brovanov, I.S.: Compressibility of Binary Mixtures of Helium, Nitrogen or Argon with Carbon Dioxide at $59 \cdot 10^5$ up to $590 \cdot 10^5$ Pa. Teploenergetika **22**(11), 87–89 (1975)

[31] Altunin, V.V., Koposhilov, O.D.: An Experimental Investigation of the Thermal Properties of Gaseous Mixtures of Carbon Dioxide with Argon. Teploenergetika **24**(8), 80–83 (1977)

[32] Mantovani, M., Chiesa, P., Valenti, G., Gatti, M., Consonni, S.: Supercritical Pressure-Density-Temperature Measurements on CO_2-N_2, CO_2-O_2 and CO_2-Ar Binary Mixtures. The Journal of Supercritical Fluids **61**, 34–43 (2012) https://doi.org/10.1016/j.supflu.2011.09.001

[33] Yang, X., Richter, M., Wang, Z., Li, Z.: Density Measurements on Binary Mixtures (Nitrogen + Carbon Dioxide and Argon + Carbon Dioxide) at Temperatures from (298.15 to 423.15) K With Pressures From (11 to 31) MPa Using a Single-Sinker Densimeter. The Journal of Chemical Thermodynamics **91**, 17–29 (2015) https://doi.org/10.1016/j.jct.2015.07.014